



OPEN ACCESS

EDITED BY

Enketeswara Subudhi,
Siksha O Anusandhan University, India

REVIEWED BY

Jae Ho Shin,
Sartorius, Germany
Zhi-Gang Jeff Qian,
Shanghai Jiao Tong University, China

*CORRESPONDENCE

Laura García-Calvo,
✉ laura.g.calvo@ntnu.no

SPECIALTY SECTION

This article was submitted to
Biochemical Engineering,
a section of the journal
Frontiers in Chemical Engineering

RECEIVED 11 January 2023

ACCEPTED 27 February 2023

PUBLISHED 13 March 2023

CITATION

García-Calvo L, Rane DV, Everson N,
Humlebrekk ST, Mathiassen LF,
Mæhlum AHM, Malmo J and Bruheim P
(2023), Central carbon metabolite
profiling reveals vector-associated
differences in the recombinant protein
production host *Escherichia coli* BL21.
Front. Chem. Eng. 5:1142226.
doi: 10.3389/fceng.2023.1142226

COPYRIGHT

© 2023 García-Calvo, Rane, Everson,
Humlebrekk, Mathiassen, Mæhlum,
Malmo and Bruheim. This is an open-
access article distributed under the terms
of the [Creative Commons Attribution
License \(CC BY\)](https://creativecommons.org/licenses/by/4.0/). The use, distribution or
reproduction in other forums is
permitted, provided the original author(s)
and the copyright owner(s) are credited
and that the original publication in this
journal is cited, in accordance with
accepted academic practice. No use,
distribution or reproduction is permitted
which does not comply with these terms.

Central carbon metabolite profiling reveals vector-associated differences in the recombinant protein production host *Escherichia coli* BL21

Laura García-Calvo^{1*}, Divyata Vilas Rane¹, Nikalet Everson¹,
Sigurd Tømmerberg Humlebrekk¹, Lise Femanger Mathiassen¹,
Astfrid Helene Morka Mæhlum¹, Jostein Malmo² and
Per Bruheim¹

¹Department of Biotechnology and Food Science, NTNU Norwegian University of Science and Technology, Trondheim, Norway, ²Vectron Biosolutions AS, Trondheim, Norway

The Gram-negative bacterium *Escherichia coli* is the most widely used host for recombinant protein production, both as an industrial expression platform and as a model system at laboratory scale. The recombinant protein production industry generates proteins with direct applications as biopharmaceuticals and in technological processes central to a plethora of fields. Despite the increasing economic significance of recombinant protein production, and the importance of *E. coli* as an expression platform and model organism, only few studies have focused on the central carbon metabolic landscape of *E. coli* during high-level recombinant protein production. In the present work, we applied four targeted CapIC- and LC-MS/MS methods, covering over 60 metabolites, to perform an in-depth metabolite profiling of the effects of high-level recombinant protein production in strains derived from *E. coli* BL21, carrying *XylS/Pm* vectors with different characteristics. The mass-spectrometric central carbon metabolite profiling was complemented with the study of growth kinetics and protein production in batch bioreactors. Our work shows the robustness in *E. coli* central carbon metabolism when introducing increased plasmid copy number, as well as the greater importance of induction of recombinant protein production as a metabolic challenge, especially when strong promoters are used.

KEYWORDS

Escherichia coli, recombinant protein production, metabolic burden, central carbon metabolism, *XylS/Pm*, mass spectrometry, targeted metabolite profiling

Abbreviations: aKG, α -ketoglutaric acid; DO, dissolved oxygen; ICit, isocitrate; LOD, limit of detection; LOQ, limit of quantitation; OD, optical density; PCA, principal component analysis; PCN, plasmid copy number; PEP, phosphoenolpyruvate; PPP, pentose phosphate pathway; RPP, recombinant protein production; TCA, tricarboxylic acid.

1 Introduction

Recombinant DNA technology is one of the pillars that have supported the progress of Biotechnology during the past 50 years. Recombinant structural proteins and enzymes have direct applications as biopharmaceuticals (hormones, cytokines, growth factors, antibodies, etc.) and in technological processes that are central to industrial fields such as food and feed, detergents, textile, paper, waste management, organic synthesis and biofuels (Kirk et al., 2002; Overton, 2014; Puetz and Wurm, 2019). The production of recombinant proteins is an expanding industry with increasing economic significance. Reports have estimated that the value for the global enzymes market in 2021 exceeded \$6 billion, and a steady growth projection is forecast for the following years, at a compound annual growth rate of 6.3%–6.8% between 2019 and 2027 (Sutay Kocabas and Grumet, 2019; BlueWeave Consulting and Research Pvt Ltd, 2021; de la Fuente et al., 2021; Espina et al., 2021; Mesbah, 2022). Concerning biopharmaceuticals, as of 2018, more than 300 protein-based drugs had been approved in Europe and United States, and almost a third of all pharmaceuticals in development were protein-based (Walsh, 2018). The market of protein-based biopharmaceuticals has only continued to grow, with numerous new drugs being approved each year (Martins et al., 2022), and global sales reaching \$90.53 billion in 2020 (Sanchez-Trasviña et al., 2021).

Obtaining these highly profitable recombinant protein-based products requires an expression platform. The range of available hosts for recombinant protein production (RPP) is extensive, including eukaryotic organisms, such as filamentous fungi, yeast, mammalian cell lines, transgenic plants, transgenic animals and insect cells, as well as prokaryotic hosts (Tripathi and Shrivastava, 2019). Among the latter, *Escherichia coli* is to this date the most widely used host for RPP (Terpe, 2006; Kaur et al., 2018; Lozano Terol et al., 2021). This Gram-negative, facultative anaerobic bacterium presents characteristics that render it an advantageous RPP expression platform. *E. coli* has unparalleled fast growth kinetics, rapid gene expression, it is relatively easy to cultivate using inexpensive substrates, it has the potential to achieve high product yields, and it can be easily genetically modified, thanks to the variety of well-established molecular tools available to edit its genome (Baneyx, 1999; Terpe, 2006; Waegeman and Soetaert, 2011; Overton, 2014; Rosano and Ceccarelli, 2014; Kaur et al., 2018). *E. coli* can be used in combination with different promoter/regulator systems to achieve high RPP yields. One such system is composed of the *Pm* promoter and its cognate regulator gene *xylS*, which originates from the *Pseudomonas putida* TOL plasmid pWW0, and plays a role in the regulation of an operon that encodes enzymes for the degradation of aromatic hydrocarbons (Worsey and Williams, 1975). Expression vectors containing the *XylS/Pm* system can be easily induced with inexpensive benzoic acid derivatives, in a dose-dependent manner, which allows tight control of the expression of recombinant genes. The *XylS/Pm* system has been used in combination with the minimal replication elements *oriV* and *trfA* from the naturally occurring RK2 plasmid, to originate

vectors that are functional in different expression hosts. The plasmid copy number (PCN) can be selected by utilizing *trfA* genes with specific point mutations. Moreover, the *XylS/Pm* expression system has been further improved in the last decades to allow for tightly controlled RPP in *E. coli* (Gawin et al., 2017).

Although *E. coli* remains one of the most prominent RPP hosts, it presents shortcomings that negatively impact product yields. High-level RPP may affect the stability of *E. coli*'s nucleic acid and impair processes such as transcription, translation, protein folding and protein translocation (Silva et al., 2012; Overton, 2014; Singha et al., 2017). Contrary to most small molecule biosynthesis, with one or few building blocks, protein biosynthesis draws carbon and energy resources from the entire central carbon metabolism, that is, the highly conserved network of interconnected pathways that permit the catabolism of sugars to obtain biosynthetic precursors in practically every known living organism. The metabolic burden imposed on *E. coli* by the maintenance of a foreign plasmid and the expression of heterologous genes can inhibit growth, affect the morphological phenotype, induce stress responses, as well as lead to metabolic alterations that affect the viability of the cell and severely reduce protein yields (Glick, 1995; Jeong and Lee, 2003; Hoffmann and Rinas, 2004; Haddadin and Harcum, 2005; Ow et al., 2006; Silva et al., 2012; Lozano Terol et al., 2021).

E. coli has been a major model system in microbiology for decades, and a plethora of works have investigated the genomic, transcriptomic, proteomic and metabolomic landscape of this bacterium (Han and Lee, 2006; Sevastyanovich et al., 2010; Guo et al., 2012; Jeong et al., 2015; Kim et al., 2017; Li et al., 2017; Kim et al., 2018). ECMDB, a dedicated database for *E. coli* metabolomic data, is established (Guo et al., 2012), but the datasets included in ECMDB are not on the preferred RPP strain BL21, and study objectives are centered on growth. Thus, despite its importance as a host, surprisingly few studies focus on the metabolic burden consequences of high-level RPP in *E. coli* from a metabolomics point of view (Weber et al., 2002; Wittmann et al., 2007; Silva et al., 2012; Mairhofer et al., 2013; Muhamadali et al., 2016; Chae et al., 2017). This knowledge gap about the wider picture of the metabolic burden associated to RPP, together with the need to obtain a product rapidly, determines that the RPP industry often adopts a “trial-and-error” strategy to optimize RPP in *E. coli*, an approach that demands intensive use of time, manpower and equipment (Sevastyanovich et al., 2010). The metabolic burden of RPP on *E. coli* has been insufficiently studied, and further work is needed in order to understand and engineer the mechanisms governing these drawbacks.

In the present work, we applied a deep phenotyping approach by means of advanced quantitative CapIC- and LC-MS/MS workflows (Kvitvang et al., 2014; Stafnes et al., 2018; Røst et al., 2020a; Røst et al., 2020b) to perform the first in-depth characterization of the metabolic burden imposed on central carbon metabolism pathways when a classical RPP strain, *E. coli* BL21, is submitted to different levels of RPP, in genetically engineered *E. coli* BL21 strains harboring different PCN and promoter strengths.

TABLE 1 Expression vector name, resulting strain abbreviation, expression cassette strength, regulator gene *trfA* variant, plasmid copy number (PCN), presence/absence of the *mCherry* gene and plasmid size of the bacterial strains used in the present work. All strains derive from the *Escherichia coli* BL21 wild-type (WT) strain. Plasmids were provided by Vectron Biosolutions AS.

Plasmid name	Strain abbreviation	Expression cassette strength ^a	<i>trfA</i> gene variant	PCN ^b	<i>mCherry</i> gene	Plasmid size (kbp)
-	WT	-	-	-	-	-
pVB-1A0A1	A1	Wild type	Wild type	+	No	8.25
pVB-1A0B1	A2	Wild type	271C mutant	++	No	8.17
pVB-1A0C1	A3	Wild type	251M mutant	+++	No	8.17
pVB-1A0D1	A4	Wild type	254D mutant	++++	No	8.17
pVB-1Z0A1	Z1	Increased ^a	Wild type	+	No	8.25
pVB-1Z0B1	Z2	Increased	271C mutant	++	No	8.25
pVB-1Z0C1	Z3	Increased	251M mutant	+++	No	8.25
pVB-1Z0D1	Z4	Increased	254D mutant	++++	No	8.25
pVB-1A0A1	A1-mCh	Wild type	Wild type	+	Yes	8.93
pVB-1A0B1	A2-mCh	Wild type	271C mutant	++	Yes	8.93
pVB-1A0C1	A3-mCh	Wild type	251M mutant	+++	Yes	8.93
pVB-1A0D1	A4-mCh	Wild type	254D mutant	++++	Yes	8.85
pVB-1Z0A1	Z1-mCh	Increased	Wild type	+	Yes	8.93
pVB-1Z0B1	Z2-mCh	Increased	271C mutant	++	Yes	8.93
pVB-1Z0C1	Z3-mCh	Increased	251M mutant	+++	Yes	8.93
pVB-1Z0D1	Z4-mCh	Increased	254D mutant	++++	Yes	8.85

^aIncreased: mutated promoter and 5'UTR; approximately 25 times stronger than wild-type.

^bPCNs, for each mutation have been discussed in previous publications (Durland et al., 1990; Haugan et al., 1995; Blatny et al., 1997; Sletta et al., 2004).

2 Materials and methods

2.1 Microorganisms and cultivation conditions

E. coli BL21 (*fhuA2 [lon] ompT gal [dcm] ΔhdsS*; New England Biolabs, Irving, MA, United States) was used as a recombinant production host. The RPP strains studied in the present work were obtained by transforming BL21 competent *E. coli* cells (C2530H, New England Biolabs, Ipswich, MA, United States) with different versions of the pVB expression vector, provided by Vectron Biosolutions AS (Trondheim, Norway). To construct the pVB expression vectors, the *mCherry* sequence was gene synthesized (Genscript, Piscataway, NJ, United States) and inserted between *NdeI-XhoI* sites in the pVB expression plasmids. The characteristics of each pVB plasmid and the resulting strains are detailed in Table 1. In strains harboring pVB plasmids, selection pressure was maintained by supplementing the media with ampicillin (100 μg mL⁻¹; A0839.0100, Panreac AppliChem, Darmstadt, Germany). Bacterial strains were stored in 16% (v/v) glycerol (24387.292, VWR, Radnor, PA, United States), at -80°C.

For initial screenings, bacterial strains were cultured in a small scale microbioreactor (BioLector Pro, m2p-labs, Aachen, Germany), monitored and controlled by BioLecture 3.18 software. Precultures were prepared by adding 100 μL of bacterial glycerol stock to 10 mL

defined mineral Hi medium in 125 mL baffled shake flasks (2543-00125, Bellco Glass, Vineland, NJ, United States), and incubated overnight (30°C, 200 rpm, 16 ± 1 h). Hi medium is a modification of the HiYe medium (Sletta et al., 2007), formulated to remove complex ingredients, and is composed as follows: 8.6 g L⁻¹ Na₂HPO₄·2H₂O (30435, Honeywell Fluka, Charlotte, NC, United States), 3 g L⁻¹ KH₂PO₄ (P5655, Sigma-Aldrich, Saint-Louis, MO, United States), 1 g L⁻¹ NH₄Cl (A9434, Sigma-Aldrich), 0.5 g L⁻¹ NaCl (27810.295, VWR), 0.62 g L⁻¹ MgSO₄·7H₂O (M5921, Sigma-Aldrich), 0.06 g L⁻¹ Fe(III) citrate hydrate (F3388, Sigma-Aldrich), 0.003 g L⁻¹ H₃BO₃ (B6768, Sigma-Aldrich), 0.015 g L⁻¹ MnCl₂·4 H₂O (M5005, Sigma-Aldrich), 0.0084 g L⁻¹ EDTA·2H₂O (E6635, Sigma-Aldrich), 0.0015 g L⁻¹ CuCl₂·2H₂O (C3279, Sigma-Aldrich), 0.0025 g L⁻¹ Na₂Mo₄O₄·2H₂O (M1651, Sigma-Aldrich), 0.0025 g L⁻¹ CoCl₂·6H₂O (C8661, Sigma-Aldrich), 0.008 g L⁻¹ Zn(CH₃COO)₂·2H₂O (379786, Sigma-Aldrich) and 20 g L⁻¹ glucose (101176K, VWR) in Milli-Q (MQ; 18.2 MΩ cm)-H₂O. Microbioreactor cultivations were carried out in FlowerPlate 48-well flower-shaped microtiter plates (m2p-labs), covered by a disposable gas-permeable adhesive membrane with evaporation reducing layer (F-GPR48-10, m2p-labs), containing 800 μL Hi medium per well. Microbioreactor cultures were initiated by inoculating from overnight precultures for a starting optical density at 600 nm (OD₆₀₀) of 0.1 in each well. Biomass (gain 6),

fluorescence (gain 10), dissolved oxygen (DO; %) and pH were recorded every 10 min. Plates were incubated at 30°C, 1,400 rpm and 85% humidity until Biomass reached 30 arbitrary units (approximately 0.7 g CDW L⁻¹); at Biomass 30, temperature was reduced to 25°C and 1 mM m-toluate was added to induce expression from the *XylS/Pm* system. Three independent replicates were cultured per strain. Calibration curves for Biomass (gain 6) values against g CDW L⁻¹ were prepared by fast filtering a volume containing an equivalent amount of biomass (5 OD₆₀₀ units) at different growth densities, through hydrated Durapore hydrophilic PVDF 0.45 µm pore size membrane disc filters with a diameter of 47 mm (HVLP04700, Merck), coupled to a filtration manifold (X516-1,038, VWR) with a magnetic filter funnel (516-7597, VWR). Vacuum was controlled by a vacuum pressure controlling unit (CVC3000 and VSK3000, Vacuubrand, Wertheim, Germany) connected to a vacuum pump (ME 4R NT, Vacuubrand). After fast filtration, filters containing cell samples for CDW were rinsed with 10 mL of MQ-H₂O at 30°C and transferred to pre-weighed aluminum pans (611-1,376, VWR) that were subsequently dried at 110°C until constant weight. CDW values for the different Biomass (gain 6) measurements were obtained by interpolation from the mentioned calibration curve.

Selected strains were grown at a larger scale in benchtop stirred tank bioreactors. Two consecutive precultures were used. Firstly, 125 µL glycerol stock were added to 250 mL baffled shake flasks (2543-00250, Bellco Glass) containing 50 mL rich LB medium, prepared dissolving 10 g L⁻¹ tryptone (T9410, Sigma-Aldrich), 5 g L⁻¹ NaCl (27810.295, VWR) and 5 g L⁻¹ yeast extract (92144, Sigma-Aldrich) in MQ-H₂O. Primary precultures were incubated for 8 h at 30°C and 200 rpm. Then, 300 µL primary preculture were added to 500 mL baffled shake flasks (2543-00500, Bellco Glass) containing 100 mL Hi medium. Secondary precultures were incubated at 30°C and 200 rpm for 12 ± 1 h, until late exponential growth phase. Bioreactor cultivations were started at OD₆₀₀ = 0.1, by adding a corresponding volume of secondary preculture to 0.9 L defined mineral Hi-F medium, composed as follows: 16 g L⁻¹ KH₂PO₄ (P5655, Sigma-Aldrich), 4 g L⁻¹ (NH₄)₂HPO₄ (101207.0500, Merck, Darmstadt, Germany), citric acid monosodium salt (447690010, Acros Organics, Geel, Belgium), 1.5 g L⁻¹ MgSO₄·7H₂O (M5921, Sigma-Aldrich), 0.075 g L⁻¹ Fe(III) citrate hydrate (F3388, Sigma-Aldrich), 0.0038 g L⁻¹ H₃BO₃ (B6768, Sigma-Aldrich), 0.0188 g L⁻¹ MnCl₂·4 H₂O (M5005, Sigma-Aldrich), 0.0105 g L⁻¹ EDTA·2H₂O (E6635, Sigma-Aldrich), 0.0019 g L⁻¹ CuCl₂·2H₂O (C3279, Sigma-Aldrich), 0.0031 g L⁻¹ Na₂Mo₄O₄·2H₂O (M1651, Sigma-Aldrich), 0.0031 g L⁻¹ CoCl₂·6H₂O (C8661, Sigma-Aldrich), 0.01 g L⁻¹ Zn(CH₃COO)₂·2H₂O (379786, Sigma-Aldrich) and 20 g L⁻¹ glucose (101176K, VWR) in MQ-H₂O. Batch bioreactor cultivations were performed in stirred glass tank autoclavable benchtop bioreactors (1 L, Applikon Biotechnology, Delft, Netherlands) controlled by my-Control units (Z310210011, Applikon Biotechnology), and equipped with AppliSens pH⁺ sensors (Z001023551, Applikon Biotechnology) and AppliSens Low Drift DO₂-sensors (Z010023525, Applikon Biotechnology). The pH was kept at 7.00 by automatically pumping 4 M NH₄OH (30501, Sigma-Aldrich). Temperature was maintained at 30°C until OD₆₀₀ = 2.5, when cultures were induced with 1 mM m-toluate. Immediately after induction with m-toluate, the temperature in the

bioreactor was lowered to 25°C. Aeration was controlled by sparging 600 mL min⁻¹ of sterile-filtered air into the bioreactors and adjusting stirring from 200 to 800 rpm to ensure levels of DO above 40%. Monitoring and logging of online cultivation data was carried out in BioXpert[®] 2 (Applikon Biotechnology). Cell growth was recorded regularly through spectrophotometric measurements of OD₆₀₀. CDW values for the different OD₆₀₀ measurements were obtained by interpolation from calibration curves for OD₆₀₀ against g CDW L⁻¹, prepared by fast filtering, as detailed above for the Biolector Pro cultivations. For online monitoring of recombinant protein production during benchtop scale bioreactor cultivations, mCherry fluorescence was evaluated in technical triplicates in a Spark 20M microplate reader (Tecan, Männedorf, Switzerland), with bottom reading at gain 66, excitation wavelength 560 nm, and emission wavelength 635 nm. mCherry concentration values were obtained by interpolation from a calibration curve prepared in triplicates from commercial pure mCherry (ABIN412973, antibodies-online GmbH, Aachen, Germany), measured in the Spark 20M Microplate reader with the parameters indicated above.

2.2 Quantification of extracellular products and substrates

Air flow, percentage (v/v) of O₂ (m/z 32) and CO₂ (m/z 44) in the exhaust gas were measured continuously by a Prima BT Bench Top Process Mass Spectrometer (ThermoFisher Scientific, Waltham, MA, United States). Samples for exometabolite analyses were collected from exponentially growing batch benchtop stirred tank bioreactor cultivations, in at least triplicates. Cultivation broth samples were centrifuged (8,000 rcf, 5 min, 4°C) to separate spent media and cells. Supernatants were subsequently transferred to clean microtubes, snap frozen in liquid nitrogen (LN₂) and stored at -80°C. Before analysis, samples were filtered through 13 mm syringe filters with a 0.2 µm pore size PTFE membrane (514-0068, VWR). D-glucose and excreted organic acids were measured using high-performance liquid chromatography (HPLC), by means of an Alliance HPLC (Waters, Millford, MA, United States of America) with a refractive index (RI) and a UV/Vis detector, and a Hi-Plex H 300 × 7.7 mm column (PL1170-6830, Agilent Technologies, Santa Clara, CA, United States), as described elsewhere (Kumar et al., 2021). Concentrations were calculated by interpolation from a standard curve prepared with commercial standards: D-glucose (101176K, VWR), acetic acid (1.00063.1011, Supelco, Bellefonte, PA, United States), lactic acid (L1500, Sigma-Aldrich) and succinic acid (S3674, Sigma-Aldrich).

2.3 Targeted mass spectrometric metabolic profiling of intracellular metabolites

2.3.1 Quantification of organic acids, amino acids, and phosphorylated metabolites

For the analysis of organic acids, amino acids and phosphorylated metabolites, exponentially growing cells were sampled by fast filtration, according to a protocol based on (Kvitvang and Bruheim, 2015), with the modifications detailed in

(Thorfinnsdottir et al., 2023). A volume corresponding to 5 units of OD₆₀₀ was collected through a bioreactor sampling port and immediately fast filtered at a vacuum pressure 800 mbar below the ambient pressure. Cells were harvested on hydrated Durapore hydrophilic PVDF 0.45 μm pore size membrane disc filters with a diameter of 47 mm (HVLP04700, Merck), as indicated in Section 2.1 of Material and Methods. Harvested cells were rinsed with 10 mL MQ-H₂O at the same temperature as the corresponding cultivation (30 or 25°C). Filters were then submerged in centrifuge tubes containing MQ-H₂O: ACN (83640.320, VWR): methanol (1.06035.2500, Merck) (5:3:2, v/v) at -20°C, for rapid quenching of metabolic reactions. Quenched samples were immediately snap frozen in LN₂ and stored at -80°C until further processing. Metabolites were extracted from quenched samples by thawing and incubating for 30 min at -20°C in a low temperature circulating bath filled with ethanol, with mixing by vortexing for 20 s every 10 min. Then, filters were carefully discarded, and the extracts were centrifuged (4,500 x g, -9°C, 10 min) to separate cell debris. Metabolites were concentrated by lyophilization (0.05 mbar, -105°C) in a SP VirTis BenchTop Pro (SP Scientific, Warminster, PA, United States of America) and reconstitution in 0.5 mL cold MQ-H₂O. To clear greater residual cell debris, reconstituted metabolite extracts were centrifuged (4,500 x g, 4°C, 5 min) and then spin filtered through 10 kDa cutoff spin filters (20,800 x g, 4°C, 10 min; 516-0230P, VWR).

Cleared cell extracts were further processed for the spectrometric quantification of intracellular amino acids, organic acids, and phosphorylated metabolites, by means of two targeted LC- and one capillary ion chromatography (CapIC) hyphenated MS/MS methods, respectively. Sample processing, derivatization (for organic acids and amino acids) and analytical protocols were carried out as detailed elsewhere (Kvitvang et al., 2014; Stafnes et al., 2018; Røst et al., 2020a). Interpolation from calibration curves elaborated with analytical grade standards (Santa-Cruz Biotechnology, Dallas, Texas, United States of America; Sigma-Aldrich) calculated by least-squares regression with 1/x weighting, and isotope dilution, were used to obtain absolute endometabolite quantifications.

2.3.2 Quantification of intracellular pyridine nucleotides

For analysis of intracellular pyridine nucleotides, a volume of cultivation broth equivalent to 5 units of OD₆₀₀ was harvested from bioreactors at exponential growth phase, in triplicates. Harvested cultivation broth was pelleted by centrifugation at 4,500 x g (5 and 15 mL centrifuge tubes) or 8,000 x g (1.5 and 2.2 mL microtubes), at 4°C, for 5 min. The supernatant collected for analysis of extracellular metabolites, and the cell pellet was immediately snap frozen in LN₂ and stored at -80°C until further sample processing. Frozen cell pellets were submitted to metabolite extraction and quantification by LC-MS/MS, as detailed in (Røst et al., 2020b).

2.4 Data Processing, Statistical Analysis, and Visualization

Cultivation data from Biolector Pro and benchtop bioreactor cultivations were plotted using Matplotlib v3.3.4 (Hunter, 2007).

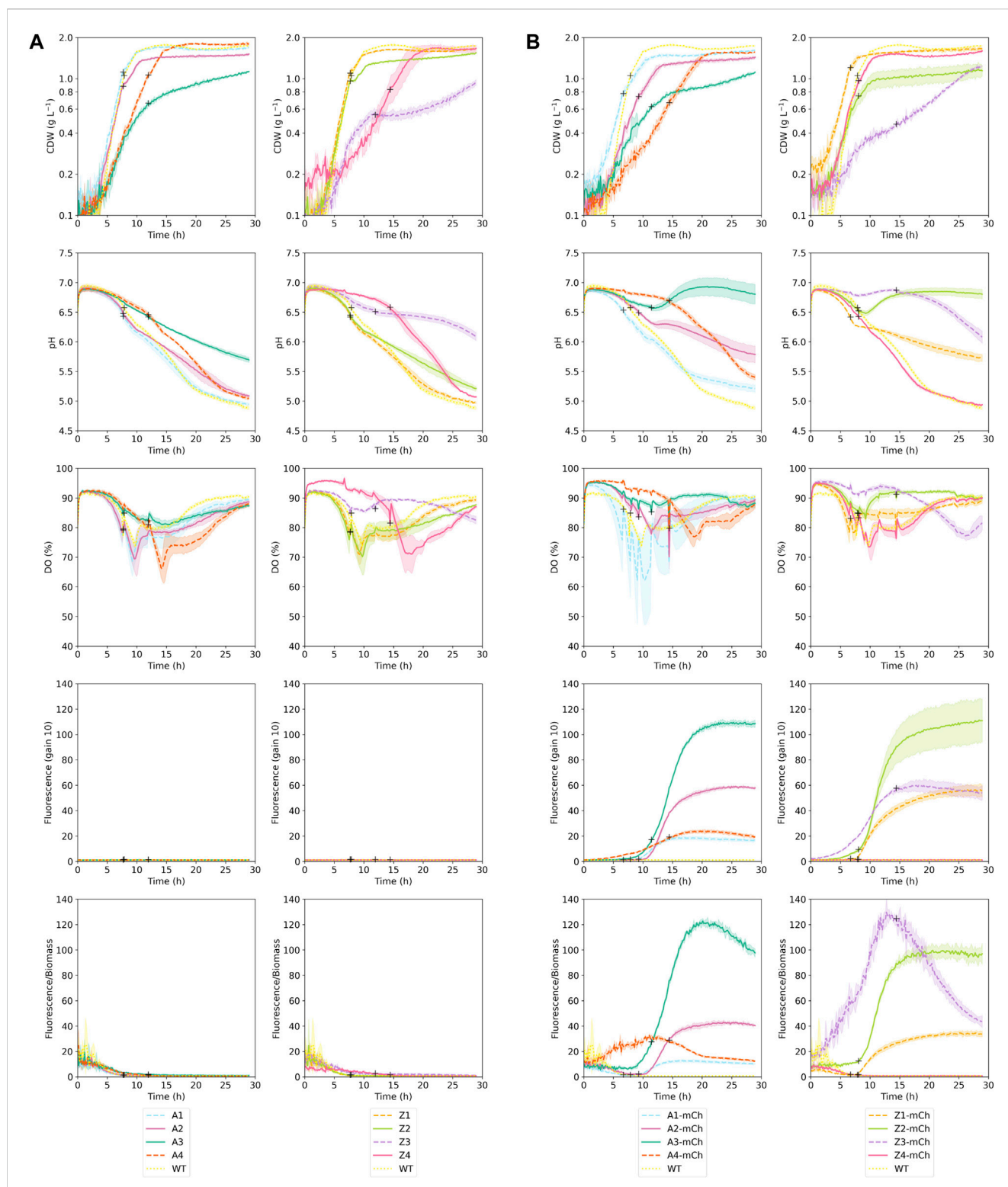
The specific growth rate, μ (h⁻¹), was calculated during exponential growth phase, as the slope of a semi-logarithmic plot of biomass concentration or OD₆₀₀ versus time. Specific rates (specific glucose uptake rate, q_s , g g⁻¹ CDW h⁻¹; specific CO₂ production rate, p_{CO_2} , mmol g⁻¹ CDW h⁻¹; and specific mCherry production rate, q_{mCh} , mg g⁻¹ CDW h⁻¹) were calculated during exponential growth phase by dividing the volumetric rate by the mean biomass between two time points. mCherry yield per substrate consumption ($Y_{mCh/s}$, mg g⁻¹) was calculated by dividing biomass or mCherry produced by the amount of glucose consumed between two time points. % Carbon recovery was calculated on a mmol/L basis, assuming 27.3 g/mol as molecular weight for the biomass, from the biomass formula CH_{1.8}O_{0.5}N_{0.2} and 10% estimated ashes (Doran, 2013); the flows considered for the mass balance equation were glucose as substrate, and biomass, CO₂, mCherry, acetic acid, lactic acid and succinic acid as products, consumed or produced between two time points.

Endometabolome data processing was performed as described in (Røst et al., 2020a), with modifications. Mass spectrometric data were inspected and processed in the TargetLynx application manager of the MassLynx 4.1 software (Waters). Absolute quantification of endometabolites was obtained interpolating from calibration curves elaborated with analytical grade standards (Santa-Cruz Biotechnology, Dallas, Texas, United States; Sigma-Aldrich) calculated by least-squares regression with 1/x weighting, and isotope dilution was used as a correction strategy. Measured concentrations in metabolite extracts obtained from the LC-MS/MS and CapIC-MS/MS analyses were corrected for the dilution and concentration steps taking place during sample processing. Corrected concentrations were normalized to CDW (g L⁻¹), obtained from cultivation samples harvested at each sampling point in similar conditions, following the fast filtration protocol detailed in Section 2.1 of Material and Methods. Two-tailed Dixon's Q tests with a 95% confidence interval were used to identify and reject potential outliers in the sub-sample sets (Dean and Dixon, 1951). The data were further visualized and submitted to statistical analysis using MetaboAnalyst 5.0 (Pang et al., 2021). Prior to PCA and two-tailed T-tests assuming equal variances (Adjusted *p*-value (FDR) = 0.05), data was autoscaled (mean-centered and divided by the square root of the standard deviation of each variable). Log₂ fold changes of average metabolite absolute concentrations were visualized into central carbon metabolic pathways using the Omix editor and modeling tool for metabolic network diagrams (Droste et al., 2011).

The adenylate energy charge (EC) was calculated from absolute metabolite concentrations with the formula (ATP + 1/2 ADP)/(AMP + ADP + ATP) (Atkinson and Walton, 1967).

3 Results and discussion

The aim of this study was to carry out an in-depth investigation of the metabolic burden on central carbon metabolism caused by high-level RPP. To do so, a total of sixteen genetically engineered *E. coli* BL21 strains harboring different promoter strengths and PCN were submitted to an initial small-scale screening in a microbioreactor. Subsequently, a selection of five strains was scaled up to benchtop cultivations in bioreactor, to further confirm the microbioreactor findings and perform a thorough metabolic study focused on central carbon metabolism.

**FIGURE 1**

Cultivation parameters obtained during Biolector Pro cultivations. The plots display biomass (g CDW L^{-1}), pH, dissolved oxygen (DO; %), absolute fluorescence detected with gain 10, and fluorescence/biomass ratios for each of the seventeen strains that were studied. The plots correspond to three independent biological replicates per strain; averages are indicated with a colored line and standard deviations (SD) are shown as a shaded area around the averages of the same color. Measurements were performed automatically every 10 min. All cultivations were carried out at 30°C , 1,400 rpm and 85% humidity until Biomass reached 30 arbitrary units (approximately 0.7 g CDW L^{-1}); at Biomass 30, temperature was reduced to 25°C and protein production was induced by adding 1 mM *m*-toluate. Protein production induction points are marked in the figure with black + signs (A) Panels correspond to strains that did not include *mCherry* gene (empty plasmid control strains) (B) panels show *mCherry*-producing strains.

TABLE 2 Summary of results from cultivations in Biolector Pro microbioreactors with WT *Escherichia coli* BL21 and the sixteen recombinant strains studied in this work. Indicated in the table are average specific growth rates (μ ; h^{-1}) at exponential phase before (pre-induction) and after (post-induction) addition of m-toluate (average \pm SD); reduction (%) in μ pre- and post-induction, referred to WT; biomass (g CDW L^{-1}) at stationary phase (average \pm SD); and time to reach stationary phase (h after inoculation).

Strain	μ pre-induction (h^{-1})	μ post-induction (h^{-1})	Reduction (%) μ pre-induction vs. WT	Reduction (%) μ post-induction vs. WT	Biomass at stationary phase (g CDW L^{-1})	Time until stationary phase (h)
WT	0.26	0.13	0.00	0.00	1.70 \pm 0.04	11
A1	0.26	0.12	0.84	12.50	1.65 \pm 0.04	11
A2	0.23	0.12	13.08	13.39	1.46 \pm 0.04	11
A3	0.09	0.04	65.15	73.59	-	Nr ^a
A4	0.09	0.11	65.07	15.03	1.78 \pm 0.03	16
Z1	0.26	0.12	0.08	7.89	1.61 \pm 0.03	11
Z2	0.24	0.09	8.82	36.24	1.42 \pm 0.07	12
Z3	0.11	0.00	57.71	102.98	-	Nr
Z4	0.04	0.12	84.51	14.06	1.64 \pm 0.09	19
A1-mCh	0.20	0.10	21.89	26.56	1.51 \pm 0.05	11
A2-mCh	0.12	0.10	54.49	25.89	1.35 \pm 0.05	13
A3-mCh	0.06	0.05	77.03	59.30	-	Nr
A4-mCh	0.05	0.09	81.33	31.32	1.55 \pm 0.02	21
Z1-mCh	0.24	0.10	7.36	26.19	1.59 \pm 0.05	9
Z2-mCh	0.13	0.07	51.88	45.46	1.02 \pm 0.14	11
Z3-mCh	0.05	0.04	82.40	70.54	-	Nr
Z4-mCh	0.20	0.05	22.24	60.04	1.49 \pm 0.04	11

^aNr, not reached.

3.1 Effect of RPP on growth kinetics and cultivation parameters

3.1.1 Strain screening in microbioreactor: Greater differences are due to PCN and RPP-Induction

Shaken microtiter plates are predominant cultivation platforms for high-throughput screening in bioprocess development (Kensy et al., 2009a). In the present work, a Biolector Pro microbioreactor system was used to carry out online monitoring of biomass, dissolved oxygen, pH, and fluorescence, without disturbing the cultures. Cultivations were initiated at a temperature of 30°C. Subsequently, simultaneously with the addition of m-toluate for induction, the cultivation temperature was reduced to 25°C. A reduction in temperature following induction of the expression of recombinant genes is a common practice in the RPP industry and was included in this study to better simulate relevant conditions. A higher cultivation temperature before induction is also frequently applied, as it increases process efficiency by shortening the non-productive phase (Larentis et al., 2014). Moreover, previous studies have found more favorable growth rates and product yields when culturing *E. coli* at a higher temperature and then reducing it for RPP induction, pointing at increased fitness of the cells in conditions like the ones in the present work. Decreasing the cultivation temperature after induction of RPP has been reported to increase protein stability, decrease aggregation, ensure proper folding, and, overall,

lead to higher product yield (Rosano and Ceccarelli, 2014; Tripathi and Shrivastava, 2019; Huang et al., 2021). RPP at higher temperatures can cause increased metabolic burden (Muhmann et al., 2017).

Growth kinetics and cultivation parameters were evaluated in Biolector Pro cultivations for wild-type (WT) *E. coli* BL21 and a total of sixteen derived recombinant *E. coli* strains: eight mCherry-producing strains, harboring either a native or increased strength promoter, with four different levels of PCN; and eight “control strains”, with similar promoters and PCN, but not carrying the *mCherry* gene (Table 1). The results of three independent biological replicates per strain cultured in Biolector Pro are shown in Figure 1, and the corresponding calculated values for specific growth rates (μ ; h^{-1}), biomass at stationary phase (g CDW L^{-1}) and elapsed cultivation time until stationary phase (h) are indicated in Table 2. As illustrated in Figure 1, pH values remained between 6.5 and 7.0 during exponential growth phase in all cultivations, which is within the optimal range for *E. coli* (Philip et al., 2018). As for aeration, the DO (%) values stayed above 50% in all cases. DO values above 30% have previously been reported as unrestricted for *E. coli* during RPP (Sharma et al., 2020), and this assumption is supported by the absence of acetate accumulation in *E. coli* B grown at 30% DO (Phue and Shiloach, 2005). The findings presented in Figure 1 indicate that the microbioreactor cultivation conditions selected in the present work were adequate to provide good aeration

in all the studied strains. The flower-shaped baffled well geometry used in our work has previously been considered optimal to ensure oxygen transfer in small-scale cultivations (Funke et al., 2009). Oxygen availability is important for protein production (Konz et al., 1998; Losen et al., 2004), especially when expressing genes for reporter proteins such as mCherry, which requires oxygen for fluorophore maturation in order to display fluorescence (Kunze et al., 2014).

As reported in Table 2, the growth kinetics for the WT *E. coli* BL21 strain (WT) and control strains without the *mCherry* gene with lowest PCN (A1 and Z1) were very similar, both concerning specific growth rates, highest biomass (g CDW L⁻¹) achieved and time to reach stationary phase. This finding suggests that, at low PCN, the maintenance of the plasmids and constitutive expression of plasmid genes conferring antibiotic resistance did not lead to considerable growth inhibition. Plasmid maintenance appeared to influence the growth kinetics of the control strains A2, A3, Z2, Z3, which displayed lower growth rates with increasing PCN. A decrease in growth rates due to maintenance of plasmid DNA in empty strains has been recently reported in other studies (Lozano Terol et al., 2021). Moreover, the effect of the increased PCN was evident on the biomass (g CDW L⁻¹) values at stationary phase in strains A2 and Z2, which were lower than for the WT (Table 2; Figure 1). PCN has been proposed by previous works as one of the main causes of the metabolic burden associated to RPP (Bentley et al., 1990; Glick, 1995; Carneiro et al., 2013), although the implications on central metabolism of *E. coli* have not been investigated in depth, and few studies have tried to engineer central pathways of this bacterium to circumvent the metabolic consequences of high PCN (Flores et al., 2004). As for promoter strength, as shown in Table 2, it did not affect the specific growth rates in the control strains not harboring the *mCherry* gene, as there were no apparent reductions in specific growth rates of A and Z control strains with identical PCN (A1 vs. Z1; A2 vs. Z2; A3 vs. Z3).

The effects of RPP and plasmid size on growth kinetics were evident when comparing growth parameters between the negative control strains and the corresponding producing strains (Table 2; Figure 1). In all cases, mCherry-producing strains harboring similar promoters and PCN displayed lower specific growth rates than their control counterparts (A1-mCh vs. A1, A2-mCh vs. A2; A3-mCh vs. A3; Z1-mCh vs. Z1; Z2-mCh vs. Z2; Z3-mCh vs. Z3). RPP imposes a large metabolic load on the cells, which can be observed as decreased growth rates (Haddadin and Harcum, 2005). Furthermore, the biomass achieved at stationary phase was also lower for the mCherry-producing strains than for their empty-plasmid counterparts. Given that the cultivation conditions and media composition were identical for all strains, this stationary phase at lower biomass may be related to an effect of RPP-derived burden on the central metabolism of the cells.

Concerning protein production, according to fluorescence measurements, absolute mCherry production was higher with increased promoter strength, at lower PCN (Z1-mCh vs. A1-mCh; Z2-mCh vs. A2-mCh). However, interestingly, the absolute fluorescence values were lower for Z3-mCh than for A3-mCh. This finding and the growth parameters displayed on Table 2, point to an increased metabolic burden in the Z3-mCh strain derived from the combination of both high PCN and stronger promoter. Z3-mCh displayed similar relative fluorescence values per biomass compared

to A3-mCh; however, the expression of the *mCherry* gene seemed to be poorly regulated for Z3-mCh, as evidenced from the basal level expression (*leaky expression*) observed before induction (Figure 1). Tightly controlled regulation of protein expression is crucial to avoid consequences to cell growth and recombinant protein yields, especially in cases where the product may be toxic for the host cells (Rosano and Ceccarelli, 2014). Strains harboring the Z mutated stronger promoter displayed higher fluorescence in the absence of inducer than A strains. Mutated *XylS/Pm* have previously been reported to have higher background expression than their wild-type counterparts (Balzer et al., 2013). The leaky expression found in Z3-mCh, together with its reduced specific growth rate, made Z3-mCh a less favorable candidate for further studies. Finally, the strains harboring the highest PCN (A4-mCh and Z4-mCh) showed lower fluorescence than strains with similar promoter strength and lower PCN, as well as low repeatability of results between cultivation runs (results not shown) and unexpectedly higher biomass yield compared to PCN 3-strain series (Figure 1; Table 2), so they were similarly excluded from further studies. High PCN vectors have been previously associated with lower recombinant protein yields than vectors with medium or low PCN, and a strategy to improve RPP can be to opt for lower PCN (Jones et al., 2000; Terpe, 2006; Silva et al., 2012; Lozano Terol et al., 2021).

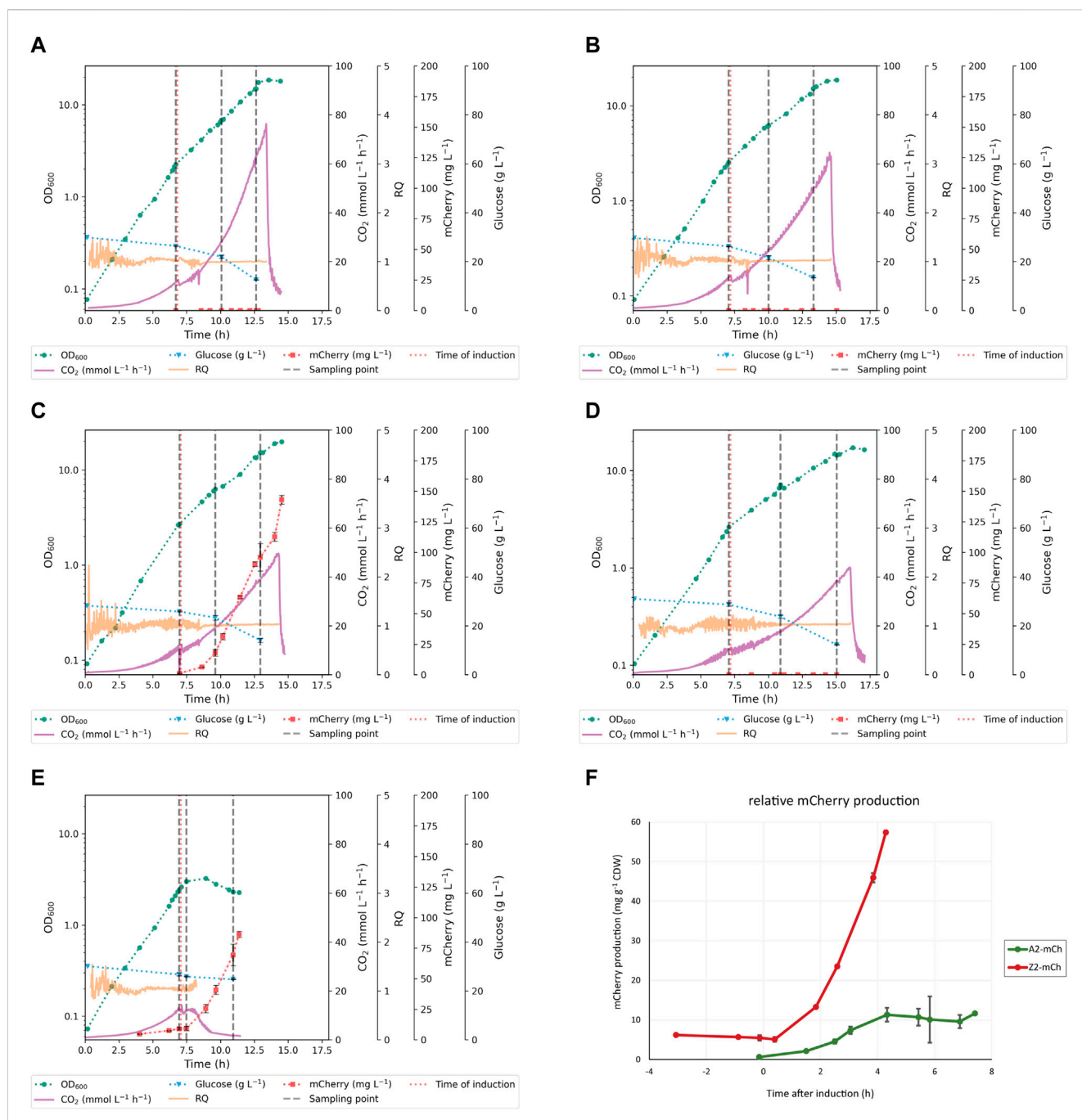
To further explore the observed differences between strains and obtain enough biomass to perform in-depth MS-based endometabolite analysis (Overton, 2014; Hemmerich et al., 2018), a selection of strains was scaled up to benchtop cultivations in bioreactor. The selected strains were A2-mCh and Z2-mCh, given that both showed altered growth kinetics in microbioreactor compared to control strains, while maintaining more tightly regulated mCherry production and high repeatability between biological replicates. The empty-plasmid counterpart strains (A2 and Z2, respectively), as well as WT *E. coli* BL21, were included as controls in the benchtop bioreactor cultivations.

3.1.2 Growth kinetics in benchtop bioreactor batch cultivations

The five selected strains (WT *E. coli* BL21, A2, A2-mCh, Z2 and Z2-mCh) were grown in Applikon benchtop bioreactors at lab scale (working volume of 0.9 L), in batch cultivations with identical conditions. In all cases, defined minimal Hi-F medium was used, starting the cultures at OD₆₀₀ 0.1, 30°C, constant air flow and adjusting agitation to maintain DO above 40% along the whole run. pH was controlled at 7.00 to ensure optimal growth conditions. RPP was induced by adding 1 mM m-toluate when the cultures reached OD₆₀₀ 2–2.5. Similarly to what was done in microbioreactor scale, the cultivation temperature was reduced to 25°C simultaneously with the addition of m-toluate for RPP induction.

3.1.2.1 Progression of the growth rate along the different cultivations

A reduction of growth rate was observed for all the studied strains after addition of the inducer, which was greater with increased promoter strength (Z versus A variant), as well as in mCherry producing strains versus their non-producing counterparts (Figures 2A–E and Table 3). Given that induction of RPP in the present study was carried out simultaneously with reduction in cultivation temperature and addition of m-toluate, the effects of these parameters on growth kinetics were assessed separately before



proceeding with the targeted endometabolite analysis. Firstly, it was confirmed that m-toluate was not toxic for the cells at the concentrations used in the present study (1 mM), and it did not alter pH, oxygen transfer nor growth kinetics in repeated cultivations of WT *E. coli* BL21 at 30°C (results not shown).

Furthermore, the effect of temperature reduction from 30°C to 25°C in absence of addition of m-toluate was assessed in the same WT control strain, as well as in the strains that displayed stronger growth rate reductions after induction: Z2 and Z2-mCh. The reduction of growth rate in Z2 and Z2-mCh following

TABLE 3 Summary of results from batch cultivations in Applikon benchtop bioreactors. The table shows the specific growth rates (μ ; h^{-1}) at exponential phase before (pre-induction) and after (post-induction) addition of m-toluate (average \pm SD); reduction (%) in μ occurred after induction in the same strain and cultivation; reduction (%) in μ pre- and post-induction, referred to WT; and biomass (g CDW L^{-1}) at stationary phase (average \pm SD).

Strain	μ pre-induction (h^{-1})	μ post-induction (h^{-1})	Reduction (%) μ after induction	Reduction (%) μ pre-induction vs. WT	Reduction (%) μ post-induction vs. WT	Biomass at stationary phase (g CDW L^{-1})
WT	0.51 \pm 0.02	0.34 \pm 0.03	33.25	-	-	10.71 \pm 0.57
A2	0.50 \pm 0.00	0.25 \pm 0.00	49.11	3.46	26.39	10.58 \pm 0.36
A2-mCh	0.49 \pm 0.02	0.25 \pm 0.01	48.42	5.09	26.65	12.12 \pm 0.14
Z2	0.47 \pm 0.00	0.20 \pm 0.01	56.84	9.08	41.20	9.15 \pm 0.18
Z2-mCh	0.48	GA	100.00	6.55	100.00	1.82 \pm 0.02

GA, growth arrest.

temperature shift from 30°C to 25°C, in absence of m-toluate, was of 34% and 33%, respectively, which is similar to that observed for WT *E. coli* BL21 (33%, as shown in Table 3). These findings confirm that the larger reduction in growth rate reported for the recombinant strains in this study can be attributed to the induction of the XylS/*Pm* system, and not to a poorer ability to adapt to lower cultivation temperatures than the WT strain. Similarly, the growth rates before induction were comparable for all five strains included in this scale-up study (Table 3; Figures 2A–E), pointing at induction of the promoter/regulator and RPP as the cause of altered growth kinetics, more than plasmid maintenance and constitutive expression of antibiotic resistance genes. Interestingly, in smaller scale experiments in microbioreactors, plasmid maintenance before induction seemed to affect growth rates in strains with high PCN and/or strong promoters, as shown in Table 2 and Figure 1. Microbioreactors constitute a very favorable initial tool for high-throughput screening and identification of general trends; however, its transferability can be suboptimal (Kensy et al., 2009a; Kensy et al., 2009b). This emphasizes the importance of complementing small-scale screenings with scale-up experiments such as the one reported in the present work, in order to better understand industrial processes and optimize small-scale approaches (Hemmerich et al., 2018).

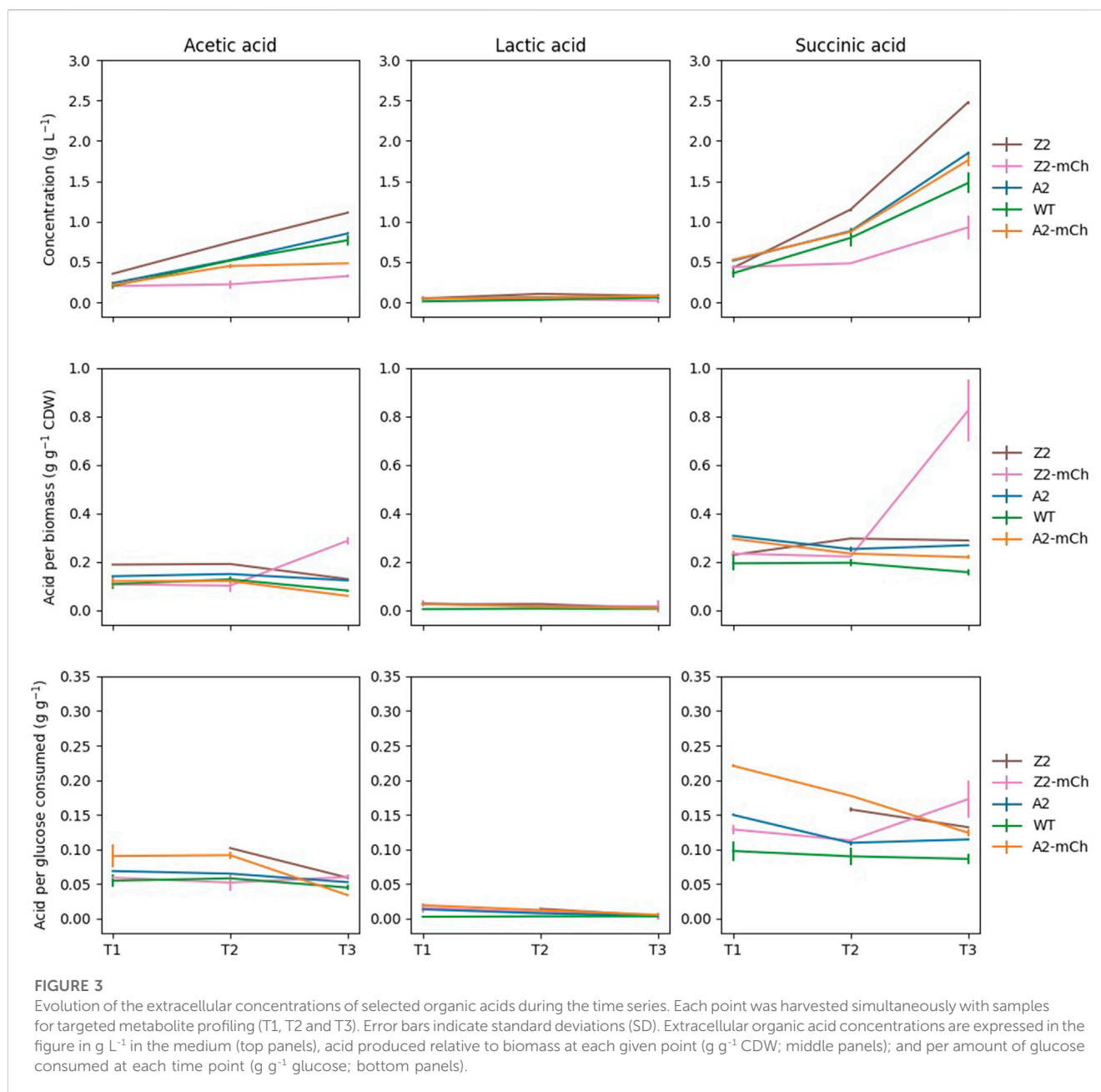
3.1.2.2 Effects of RPP on other cultivation parameters

The respiratory quotient (RQ), defined as the ratio of the carbon dioxide production to the oxygen consumption (Roels, 1981), was calculated for all strains during exponential phase. In all cases, the RQ stayed around a value of 1, which is within the expected values for growth on glucose as sole carbon source in fully aerobic conditions (Korz et al., 1995; Fan et al., 2005; Taymaz-Nikerel et al., 2010). The cultures did not enter oxygen limitation throughout the period of study (Figures 2A–E). The CO₂ evolution profile displayed similar trends in all strains but Z2-mCh, with a brief adaptation period after lowering of temperature and RPP induction (immediately after sampling point T1), followed by subsequent increase in production rate with time, until stationary phase triggered by a nitrogen limitation, when an expected drop in CO₂ production rate occurred (Figures 2A–D). As shown in Supplementary Table S2, the specific CO₂ production rate (p_{CO_2}) showed no significant differences between the WT, A2, A2-mCh and

Z2 strains at each studied time interval. On the other hand, the Z2-mCh strain entered an RPP-induced growth arrest around 30 min–1 h after induction, which was coupled with a progressive decrease in CO₂ production rate, as shown in the cultivation plots (Figure 2E) and calculated p_{CO_2} (Supplementary Table S2), especially at later time points in the production phase (T2-T3 and T1-T3). This apparent growth arrest was surprising, as Z2-mCh grew well after induction in the Biolector cultivation format, and shows a cultivation condition scale dependency of the phenotype in this strain. Growth arrest can be a consequence of the metabolic burden and maladaptation to RPP (Sevastyanovich et al., 2010; Lempp et al., 2020), and has been described for other *E. coli* strains upon rapid increase of heterologous gene expression (Haddadin and Harcum, 2005; Özkan et al., 2005; Weber et al., 2021). Although cell growth was apparently halted in Z2-mCh due to a metabolic change to accommodate the production of recombinant mCherry, the detected levels of mCherry continued to increase (Figure 2E), and the ratio of protein production per biomass was higher than for A2-mCh (Figure 2F). These findings suggest that RPP in our study was not linked to cell growth. Few studies focus on RPP in *E. coli* during stationary phase (Ou et al., 2004; Lempp et al., 2020), and further investigations could be of interest.

3.1.2.3 Production of mCherry and overflow metabolites

The consumption of glucose, as well as the production of several secreted organic acids, were evaluated by means of HPLC (Figure 3). All the strains used in the present work derive from an *E. coli* strain (BL21) that belongs to the B line, which is of high industrial relevance and the preferred one for RPP (Bernal et al., 2016). This particular strain is deficient in proteases Lon and OmpT, among other advantageous features for RPP, and has been reported to produce less overflow metabolites than K12 *E. coli* strains, which secrete more acetate (Rosano et al., 2019). Overflow metabolism occurs as a response to specific metabolic conditions, such as anaerobiosis or increased demand of precursors for biosynthesis or energy conservation (Veit et al., 2007). As it affects cell fitness, inhibits growth and biosynthesis, and consumes carbon equivalents that could instead be used to synthesize the product of interest, overflow metabolism is usually detrimental for RPP (Bernal et al., 2016). The acetate



levels produced per biomass in our study were, in general, low and comparable for all strains, except Z2-mCh, which displayed higher levels at the last time point (T3). Acetate could be excreted in this case due to a metabolic readjustment following growth arrest and RPP. Acetate production has also been hypothesized to be linked in some cases to less available membrane surface to perform oxidative energetic metabolism (Szenk et al., 2017). Z2-mCh displayed altered morphological phenotypes at T3, with significant elongation and evident filamentation (data not shown), which may contribute to this. Finally, Z2-mCh presented increased levels of succinate at T3.

The differential patterns observed in the growth kinetics, substrate consumption and product accumulation of the selected

strains were further explored by means of a comprehensive targeted endometabolite analysis.

3.2 Mass spectrometric profiling of central intracellular metabolite pools during RPP

Over 60 metabolites involved in the glycolysis, PPP and TCA central metabolic pathways, as well as nucleoside phosphates, amino acids and coenzymes participating in redox processes, were quantified in the mCherry producing recombinant strains A2-mCh and Z2-mCh, and in their non-producing control strains WT *E. coli* BL21, A2 and Z2. Three cultivation points with

equivalent biomass were collected for each strain and biological replicate. All sampling points corresponded to exponential growth phase; T1 before induction of the production of protein, and T2 and T3 after induction and establishment of protein production in the mCherry strains. For Z2-mCh, the sampling points were selected differently, adapting to the growth kinetics shown in Figures 2A–E. For this strain, T2 was collected 30 min after induction, to better capture the metabolic changes occurring after induction, before RPP-triggered growth arrest. Finally, T3 in Z2-mCh was collected at a similar time after induction as for T2 in its corresponding empty-plasmid control strain Z2, to avoid sampling well into death phase. Metabolites were absolutely quantified by means of four targeted CapIC- and LC-MS/MS methods optimized for their different physiochemical characteristics. Relative quantification of metabolites or metabolic classes is highly useful to identify changes between conditions and to obtain a general overview of the trends in metabolite pools. However, in many cases, a relative depiction is not enough to understand the metabolic landscape of a given condition. In this regard, absolute metabolite quantification provides key information necessary, for instance, to study the thermodynamics of metabolic reactions, occupation of enzymes binding-sites and to determine relevant concentration ranges for experiments (Lu et al., 2017; Røst et al., 2020a). In the present work, absolute intracellular metabolite concentrations were reported for all measured metabolites in each of the studied strains, along a time series. Absolute concentrations were obtained by interpolating from external standard calibration curves, with isotope dilution correction using labelled internal standards, and accounting for matrix effects.

3.2.1 Characteristics of the expression vector affect the relative distribution of central metabolite classes after induction of RPP

To obtain an initial general overview of the metabolic state of each strain during the time series, the relative contribution of each metabolite class to the total analyzed pool of metabolites was studied. At sampling point T1, the relative distribution by pathway and metabolite type was maintained across all the strains (Figure 4A). After induction with m-toluate and lowering of the temperature (sampling points T2 and T3), the relative distribution differed for some of the studied strains. Said greater differences with increasing time point were also evident after performing an unsupervised principal component analysis (PCA) of the averages of each strain and time point, whose 2D scores plot indicated a closer clustering at T1, with increasing spread between strains at T2, along principal components PC1 and PC2. This spread was even more accentuated at T3 (Figure 4B). These results suggest different rearrangement patterns of central carbon metabolite pools as a response to the induction of the Xyls/Pm system.

At T2, most of the strains presented similar percentual ratios, with two exceptions. Firstly, Z2-mCh T2 displayed a larger relative contribution of pyridine nucleotides. Secondly, and perhaps more importantly, A2-mCh T2 showed a markedly different distribution among several of the metabolite groups: namely, this strain presented a larger relative contribution of metabolites involved in glycolysis, PPP and nucleoside phosphates than the rest. Finally, the contribution of different metabolite classes at T3 was fairly conserved between strains, except for in the case of those

harboring the plasmids with the mutated strong promoter (Z2 and Z2-mCh). Compared to the rest of the strains, *E. coli* Z2 displayed a significantly greater proportion (%) of amino acids out of the total metabolite pool at T3 (Figure 4A), indicating that, even in the absence of a recombinant product gene, plasmid maintenance and induction with m-toluate already altered central carbon metabolism in cells harboring strong promoters and multiple PCN, something that was not observed in the control strain with equivalent PCN but weaker promoters (A2). A transcriptomic study comparing WT *E. coli* MG1655 and a recombinant strain without addition of inducer found higher expression of genes related to, among others, ATP synthesis, TCA cycle, ribosomes and amino acid synthesis, indicating metabolic effects due to plasmids, independent of RPP (Haddadin and Harcum, 2005). Finally, Z2-mCh showed a prominent relative increase in TCA cycle metabolites and decrease in glycolytic metabolites and nucleoside phosphates. These findings pointed at interesting differences in central metabolite pools during the studied conditions, which were further explored individually.

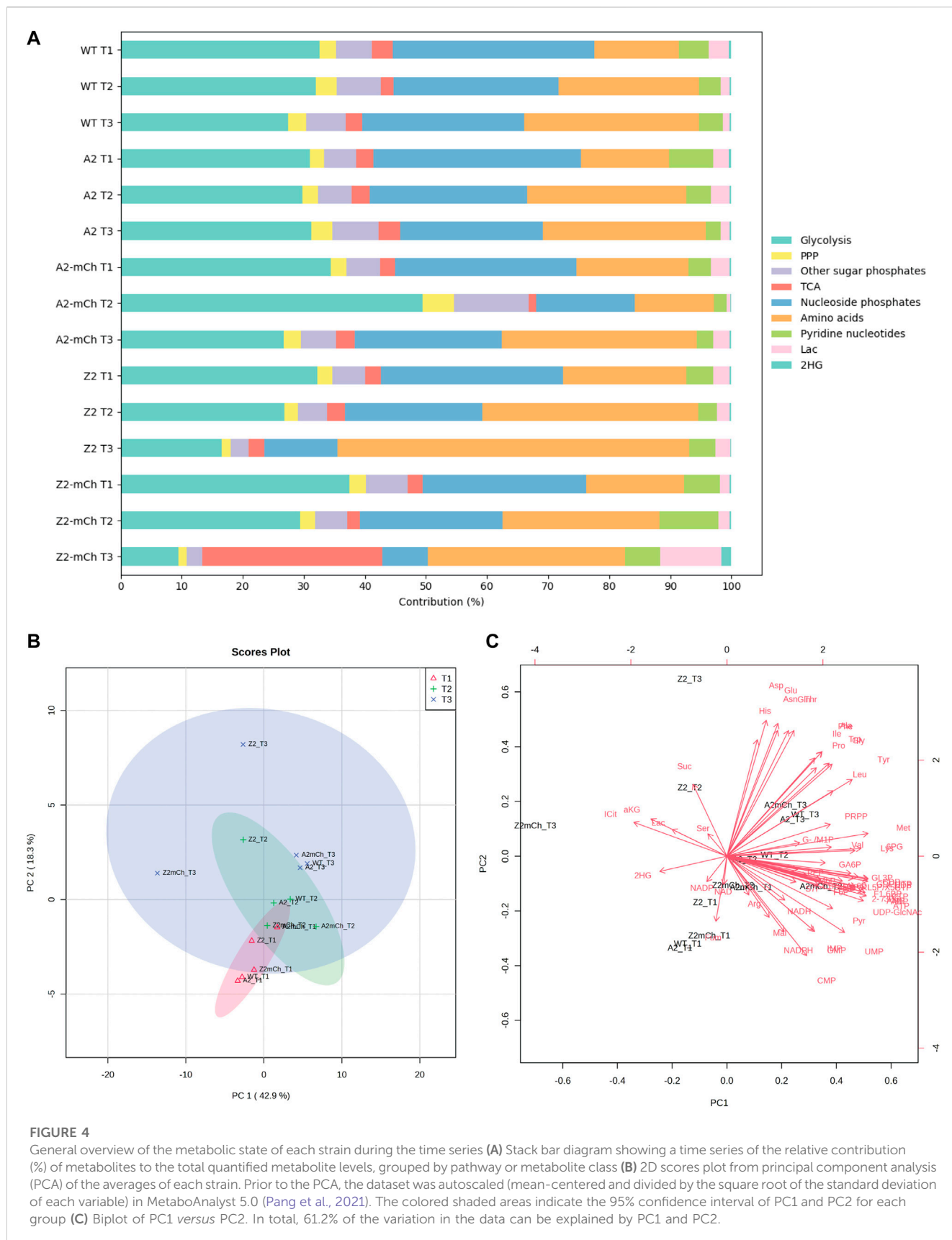
3.2.2 Absolute quantification of central metabolites and relative changes in single metabolites reveal differential metabolic responses to RPP

3.2.2.1 Overall trends

After the comparative analysis of metabolite classes among strains, the metabolomics data was subsequently inspected at individual metabolite pools level. The individual metabolite pool sizes were spanning over four orders of magnitude (Figure 5A). Furthermore, the absolute intracellular metabolite concentrations of glycolytic, PPP, nucleoside phosphates, TCA cycle intermediaries, amino acids, pyridine nucleotides and lactate were quite similar for each time point among all strains, with only one exception (Z2-mCh at the last sampling point, T3). From the overall metabolic picture of A2 and Z2, it could be inferred that the metabolite pool sizes were quite homeostatic compared to WT, with a slight reduction in several metabolite class pools at T3 for Z2 (Figure 5B). PCN was approximately 20 for the 2-series strains (A2, A2-mCh, Z2 and Z2-mCh) (Durland et al., 1990), which represents a small fraction of the total DNA content of the cells (around 3.6% and 3.9%, for empty plasmid and mCherry strains, respectively). The genomic DNA content itself constitutes only 1%–3% of the *E. coli* dry weight cell mass (Neidhardt et al., 1990; Beck et al., 2018; Simensen et al., 2022). Thus, the additional 20 plasmid copies should not cause a major precursor and energetic burden for *E. coli* before induction of heterologous gene expression, as supported by both the metabolite profiling and the cultivation data of this study (Figure 2; Table 3; Figure 5). Introducing mCherry production, however, influenced the metabolite pool distributions. The two mCherry producing strains are further evaluated in detail in the following two paragraphs.

3.2.2.2 A2-mCh

A2-mCh showed a unique metabolite profile compared to the other studied strains. At the first sampling point after induction (T2), A2-mCh presented a transient response with accumulation of glycolytic, PPP and other phosphorylated metabolites. Interestingly, at T3, A2-mCh returned to metabolite concentrations similar to what was observed for WT *E. coli* BL21 (Figure 5). From T1 to T3, A2-mCh cultures consumed approximately 11.8 g glucose L⁻¹ and



the cell density increased with 12 OD units, which amounts to approximately 7 g CDW L⁻¹. In comparison, the mCherry production was small, around 140 mg L⁻¹. This represents 4% of the precursor and energetic resources needed for protein synthesis (assuming 50% protein in *E. coli* (Simensen et al., 2022)), and 2% of the total resources for cell growth. Compared with its empty-plasmid control (A2), the glucose consumption for A2-mCh was lower between T1 and T2 (Figure 2), and the lower glycolytic flux is manifested by the metabolite accumulation at T2. These findings indicate that the induction of RPP mediated a transient stress in the cells that was resolved at the last time point T3, where the high glucose consumption was resumed. In the case of A2-mCh, we did not find the accumulation of ICit and aKG observed for Z2-mCh at a similar time after induction (T3), discussed in the next paragraph. These features, as well as the slight increase in NADPH and absence of relative decrease in amino acid pools, suggest a better adaptation to RPP in this strain (weaker promoter) as opposed to Z2-mCh (stronger promoter). These findings point to A2-mCh being a strain capable of upregulating pathways that produce energy and reducing power for anabolism (NADPH) in a more balanced manner. This fine balance can be complicated to achieve, as indicated in recent works pointing at aggravated metabolic burden due to RPP when recombinant strains accelerate the glycolytic pathway as a response to induction (Weber et al., 2021). In the present work, however, as mentioned above, we showed that A2-mCh could better adjust its central carbon metabolism to support RPP, as evidenced by the fewer relative changes in metabolite concentrations versus WT *E. coli* BL21 at the last time point (T3) (Figure 5B). Its successful adaptation to RPP was also supported by the growth kinetics depicted in Figure 2, the growth rates indicated in Table 3, and the representation of central carbon metabolism at production phase sampling points vs. Z2-mCh (Supplementary Figure S4).

3.2.2.3 Z2-mCh

Induction of mCherry production with the stronger promoter caused the complete cessation of growth in Z2-mCh, switching the cultures into a resting stationary condition with almost no glucose consumption (Figure 2), and resulting in overall metabolite pools depletion (Figure 5). However, the cells were able to maintain an mCherry production at almost the same absolute level as A2-mCh, and even a higher specific production (Figure 2F). In this regard, the yield of mCherry on glucose in Z2-mCh was 4–6 times higher than in A2-mCh, and Z2-mCh was able to convert approximately 5% (w/w) of glucose in the product mCherry, as opposed to values below 1% in A2-mCh (Supplementary Table S2). As for the metabolic profile of this strain, Z2-mCh displayed a generalized lower concentration of most metabolites, which contributed to separate this strain at T3 along PC1 in the PCA carried out for the averages of each strain (Figures 4B–C). The higher levels of ICit and aKG at T3 explain the larger relative contribution (%) of the TCA cycle indicated for this strain and time point in Figure 4A. Moreover, the terminal glycolytic intermediary phosphoenolpyruvate (PEP) was depleted, a finding recently reported for other *E. coli* strains during IPTG-induced production of hFGF-2 (Weber et al., 2021). An increase in aKG has been shown in *E. coli*, together with a depletion of PEP, during nitrogen limitation (Doucette et al., 2011), which was not present in our case. It can be speculated that the general amino acid depletion observed for Z2-mCh

T3 corresponded to a reduced biosynthetic flow from their precursors. The amino acids that showed the most marked relative decrease were valine (Val), glutamine (Gln) and asparagine (Asn). The relative composition of mCherry presents 6.4% Val, 3.4% Gln and 3% Asn, according to the ProtParat tool in ExPasy (Duvaud et al., 2021), so RPP does not necessarily explain the depletion of these amino acids in particular. As for the redox state of Z2-mCh during RPP, the log₂ fold change calculations at T2 indicated a relative increase in pyridine nucleotides involved in anabolic pathways (NADP, NADPH), with a subsequent marked depletion of NADPH and moderate reduction of NADH in the last time point (T3). The decrease in reduced pyridine nucleotides (NADH, NADPH) during higher anabolic activity, possibly related to RPP, can also be explained by the lower activity of glycolysis and PPP in this strain and time point, as indicated in Figure 5B. Another unique finding in Z2-mCh was the relative larger contribution of lactate to the total metabolite pools, as shown in Figure 4A; Figures 4C, 5B. In *E. coli*, lactate can be biosynthesized from pyruvate (Pyr), catalyzed by three lactate dehydrogenases (LDH) (Clark, 1989), and is a fermentative solution to regenerate NAD from NADH if electron transport and oxidative phosphorylation is impaired. As a summary of the findings concerning the Z2-mCh strain in the present work, the induction of RPP led to an early apparent stationary phase with growth arrest, marked differences in the total intracellular metabolite pools and individual endometabolites, as well as phenotypic and morphological changes, while still showing the highest specific mCherry production rate. RPP can trigger energetic inefficiency and undesirable physiological changes, as reported in previous studies (Wu et al., 2016).

3.2.2.4 Energy charge

The ratios of ATP, ADP and AMP can be functionally more important than the absolute concentration of ATP, and this relationship may be explored through indices such as the EC. The EC index was proposed in 1967 by Atkinson, and defined as $([ATP] + 0.5 [ADP]) / ([ATP] + [ADP] + [AMP])$ (Atkinson and Walton, 1967). In the present work, the EC was calculated for all strains and time points. All conditions except for Z2-mCh T3 did not present statistically significant differences in their calculated EC values. Z2-mCh at T3, in turn, showed a significantly lower EC (Table 4). The EC can serve as an indication of the energetic state of a cell. EC values of 0.7–0.95 have been previously reported as physiological under optimal growth conditions for a variety of organisms (De la Fuente et al., 2014; Röst et al., 2020a). The EC values reported in the present work, although slightly lower, were close to said physiological range, with the exception of Z2-mCh at sampling point T3. For Z2-mCh T3, the lower EC could be attributed to the metabolic burden derived from RPP, and it may also serve as an indication of the energetic state associated with the growth arrest experienced shortly after RPP induction. In this regard, Wittman et al., reported a reduction in EC from 0.85 to 0.6 with the onset of RPP (Wittmann et al., 2007). EC values close to our experimental results have been previously found for a K12 *E. coli* strain in an IPTG induced fed-batch culture maintained at a low growth rate and high rate of recombinant expression (Sandén et al., 2003). Furthermore, recombinant *E. coli* K12 strains have been shown to

TABLE 4 Average adenylate energy charge (EC) \pm standard deviation (SD) for each strain and sampling point, cultivated in defined mineral medium in benchtop bioreactors. Significance levels for multiple comparisons from one-way ANOVA with Tukey's HSD multiple comparisons tests are marked as ns: not significant; ***: $p \leq 0.001$.

Strain	Sampling point	Average EC \pm SD	
WT	T1	0.67 \pm 0.01	ns
	T2	0.67 \pm 0.02	ns
	T3	0.66 \pm 0.01	ns
A2	T1	0.67 \pm 0.02	ns
	T2	0.65 \pm 0.03	ns
	T3	0.65 \pm 0.04	ns
Z2	T1	0.65 \pm 0.02	ns
	T2	0.68 \pm 0.01	ns
	T3	0.67 \pm 0.00	ns
A2-mCh	T1	0.67 \pm 0.00	ns
	T2	0.66 \pm 0.00	ns
	T3	0.66 \pm 0.00	ns
Z2-mCh	T1	0.66 \pm 0.04	ns
	T2	0.66 \pm 0.01	ns
	T3	0.48 \pm 0.03	***

maintain constant EC when well-adjusted after induction of RPP (Weber et al., 2021).

To ensure the efficiency of RPP, it is important that the cell maintains high fluxes through energetic pathways, such as glycolysis, TCA cycle and the subsequent oxidative phosphorylation (Haddadin and Harcum, 2005). Recent studies on recombinant B and K12 *E. coli* strains have reported that the growth inhibitory effect of RPP may not be due to elevated energy and precursor withdrawal for plasmid related functions, but to the accumulation of catabolites and insufficient withdrawal for anabolic purposes (Li and Rinas, 2021; Weber et al., 2021). In these works, the authors found that the availability of ATP was not a limiting factor for RPP. Our results are in alignment with this finding, as the absolute intracellular concentrations of ATP remained at similar levels, except for the time point corresponding to growth arrest (Z2-mCh, T3).

3.2.2.5 Strategies to improve protein production

Several approaches could in principle be applied to improve protein productivity and alleviate the metabolic burden derived from RPP, including genetic engineering of key enzymes involved in the affected pathways, and modifications of the cultivation conditions. A limited number of studies have focused on engineering central carbon metabolic pathways in *E. coli* to improve growth kinetics or product yields by alleviating the consequences of the metabolic burden imposed by RPP (Chou, 2007; Liu et al., 2015). In this regard, Flores et al. reported a partial recovery in growth rate through engineering of the pentose phosphate pathway by modulation of the *zwf* gene expression

level, as a strategy to overcome a bottleneck in the supply of building blocks (Flores et al., 2004). This strategy could be beneficial for the Z2-mCh strain studied in the present work, given that increased concentrations of PPP metabolites were observed in A2-mCh during RPP, and this was a producing strain that did not undergo growth arrest. Redirecting and increasing the carbon flux through the oxidative branch of the PPP may help meet the demand for biosynthetic precursors and reducing power under RPP (Flores et al., 2004). In another study, Kim et al. showed that *E. coli* overexpressing phosphoenolpyruvate carboxykinase produced larger product yields with lower biomass increase than a control strain (Kim et al., 2012). Z2-mCh showed ATP depletion at late RPP sampling points (T3), and an increase in phosphoenolpyruvate carboxykinase activity could contribute to higher ATP availability. Finally, cultivation adjustments can be considered to alleviate the metabolic burden imposed on the producing strains. For instance, amino acid supplementation in the culture medium has been proven to reduce the cellular stress due to RPP and increase process productivity (Kumar et al., 2020). A generalized depletion in the amino acid concentrations was observed in the Z2-mCh strain during RPP. Given the importance of amino acids as building blocks, as well as the role of amino acid starvation during the stringent stress response, amino acid supplementation could potentially improve productivity in Z2-mCh.

3.2.2.6 Final remarks and conclusions

The metabolic burden caused by RPP has only been partially studied in *E. coli* as a host, especially with respect to the effects on central carbon metabolism. In this regard, the present study contributes to the field with, to the best of our knowledge and to this date, the most comprehensive metabolite profiling of strains harboring expression vectors with different features, and over different time points with respect to induction. Our work shows the robustness in *E. coli* central metabolism when introducing high copy number plasmids, as well as the greater importance of RPP induction as a metabolic challenge, especially when strong promoters are used.

Data availability statement

The original contributions presented in the study are included in the article/Supplementary Material, further inquiries can be directed to the corresponding author.

Author contributions

Conceptualization, LG-C, JM, and PB; Methodology, LG-C and PB; Validation, LG-C, DR, NE, SH, LM, AM, and PB; Formal Analysis, LG, DR, NE, SH, LM, AM, and PB; Investigation, LG-C, DR, NE, SH, LM, and AM; Resources, JM and PB; Writing—Original Draft Preparation, LG-C and PB; Writing—Review and Editing, LG-C and PB; Visualization, LG-C, NE, SH, LM, AM; Supervision, LG-C and PB; Project Administration, LG-C and PB; Funding Acquisition, LG-C and PB. All authors contributed to manuscript revision, read, and approved the submitted version.

Funding

This research was funded by internal funding from NTNU: The Department of Biotechnology and Food Science and the Faculty of Natural Science, as well as by the Research Council of Norway funded research-based innovation centre in Industrial Biotechnology (SFI IB, www.sfi-ib.com; project number 309558). The funders had no role in study design, data collection and analysis, decision to publish, or preparation of the manuscript.

Acknowledgments

The authors acknowledge the administrative and technical support from the host Department and the NTNU Natural Science faculty Mass Spectrometry laboratory. We especially thank senior engineer Kåre Andre Kristiansen for technical support. The authors would like to express their gratitude to Vectron Biosolutions AS for providing the strains used in this work and for their help throughout the project. Finally, we want to specially thank Lisa Marie Røst for her support with endometabolite profiling, and Emil Karlsen for his assistance and guidance using python for data visualization.

References

- Atkinson, D. E., and Walton, G. M. (1967). Adenosine triphosphate conservation in metabolic regulation. *J. Biol. Chem.* 242 (13), 3239–3241. doi:10.1016/s0021-9258(18)95956-9
- Balzer, S., Kucharova, V., Megerle, J., Lale, R., Brautaset, T., and Valla, S. (2013). A comparative analysis of the properties of regulated promoter systems commonly used for recombinant gene expression in *Escherichia coli*. *Microb. Cell Fact.* 12, 26. doi:10.1186/1475-2859-12-26
- Baneyx, F. (1999). Recombinant protein expression in *Escherichia coli*. *Curr. Opin. Biotechnol.* 10 (5), 411–421. doi:10.1016/s0958-1669(99)00003-8
- Beck, A., Hunt, K., and Carlson, R. (2018). Measuring cellular biomass composition for computational biology applications. *Processes* 6 (5), 38. doi:10.3390/pr6050038
- Bentley, W. E., Mirjalili, N., Andersen, D. C., Davis, R. H., and Kompala, D. S. (1990). Plasmid-encoded protein: The principal factor in the “metabolic burden” associated with recombinant bacteria. *Biotechnol. Bioeng.* 35 (7), 668–681. doi:10.1002/bit.260350704
- Bernal, V., Castano-Cerezo, S., and Canovas, M. (2016). Acetate metabolism regulation in *Escherichia coli*: Carbon overflow, pathogenicity, and beyond. *Appl. Microbiol. Biotechnol.* 100 (21), 8985–9001. doi:10.1007/s00253-016-7832-x
- Blatny, J. M., Brautaset, T., Winther-Larsen, H. C., Karunakaran, P., and Valla, S. (1997). Improved broad-host-range RK2 vectors useful for high and low regulated gene expression levels in gram-negative bacteria. *Plasmid* 38 (1), 35–51. doi:10.1006/plas.1997.1294
- BlueWeave Consulting and Research Pvt Ltd (2021). Global industrial enzymes market projected to reach worth \$9.2 bn by 2027. *Focus Catal.* 2021 (12). doi:10.1016/j.focat.2021.11.004
- Carneiro, S., Ferreira, E. C., and Rocha, I. (2013). Metabolic responses to recombinant bioprocesses in *Escherichia coli*. *J. Biotechnol.* 164 (3), 396–408. doi:10.1016/j.jbiotec.2012.08.026
- Chae, Y. K., Kim, S. H., and Markley, J. L. (2017). Relationship between recombinant protein expression and host metabolome as determined by two-dimensional NMR spectroscopy. *PLOS ONE* 12 (5), e0177233. doi:10.1371/journal.pone.0177233
- Chou, C. P. (2007). Engineering cell physiology to enhance recombinant protein production in *Escherichia coli*. *Appl. Microbiol. Biotechnol.* 76 (3), 521–532. doi:10.1007/s00253-007-1039-0
- Clark, D. P. (1989). The fermentation pathways of *Escherichia coli*. *FEMS Microbiol. Lett.* 63 (3), 223–234. doi:10.1111/j.1574-6968.1989.tb03398.x
- De la Fuente, I. M., Cortes, J. M., Valero, E., Desroches, M., Rodrigues, S., Malaina, I., et al. (2014). On the dynamics of the adenylate energy system: Homeorhesis vs homeostasis. *PLoS One* 9 (10), e108676. doi:10.1371/journal.pone.0108676

Conflict of interest

JM was employed by Vectron Biosolutions AS.

The remaining authors declare that the research was conducted in the absence of any commercial or financial relationships that could be construed as a potential conflict of interest.

Publisher's note

All claims expressed in this article are solely those of the authors and do not necessarily represent those of their affiliated organizations, or those of the publisher, the editors and the reviewers. Any product that may be evaluated in this article, or claim that may be made by its manufacturer, is not guaranteed or endorsed by the publisher.

Supplementary material

The Supplementary Material for this article can be found online at: <https://www.frontiersin.org/articles/10.3389/fceng.2023.1142226/full#supplementary-material>

- de la Fuente, M., Lombardero, L., Gomez-Gonzalez, A., Solari, C., Angulo-Barturen, I., Acera, A., et al. (2021). Enzyme therapy: Current challenges and future perspectives. *Int. J. Mol. Sci.* 22 (17), 9181. doi:10.3390/ijms22179181
- Dean, R. B., and Dixon, W. J. (1951). Simplified statistics for small numbers of observations. *Anal. Chem.* 23 (4), 636–638. doi:10.1021/ac60052a025
- Doran, P. M. (2013). *Bioprocess engineering principles*. Oxford, UK: Academic Press, Elsevier.
- Doucette, C. D., Schwab, D. J., Wingreen, N. S., and Rabinowitz, J. D. (2011). α -ketoglutarate coordinates carbon and nitrogen utilization via enzyme I inhibition. *Nat. Chem. Biol.* 7 (12), 894–901. doi:10.1038/nchembio.685
- Droste, P., Miebach, S., Niedenfuhr, S., Wiechert, W., and Noh, K. (2011). Visualizing multi-omics data in metabolic networks with the software Omix: A case study. *Biosystems* 105 (2), 154–161. doi:10.1016/j.biosystems.2011.04.003
- Durland, R. H., Toukdarian, A., Fang, F., and Helinski, D. R. (1990). Mutations in the *trfA* replication gene of the broad-host-range plasmid RK2 result in elevated plasmid copy numbers. *J. Bacteriol.* 172 (7), 3859–3867. doi:10.1128/jb.172.7.3859-3867.1990
- Duvaud, S., Gabella, C., Lisacek, F., Stockinger, H., Ioannidis, V., and Durinx, C. (2021). Expaty, the Swiss bioinformatics resource portal, as designed by its users. *Nucleic Acids Res.* 49 (W1), W216–W227. doi:10.1093/nar/gkab225
- Espina, G., Munoz-Ibacache, S. A., Caceres-Moreno, P., Amenabar, M. J., and Blamey, J. M. (2021). From the discovery of extremozymes to an enzymatic product: Roadmap based on their applications. *Front. Bioeng. Biotechnol.* 9, 752281. doi:10.3389/fbioe.2021.752281
- Fan, D. D., Luo, Y., Mi, Y., Ma, X. X., and Shang, L. (2005). Characteristics of fed-batch cultures of recombinant *Escherichia coli* containing human-like collagen cDNA at different specific growth rates. *Biotechnol. Lett.* 27 (12), 865–870. doi:10.1007/s10529-005-6720-8
- Flores, S., de Anda-Herrera, R., Gosset, G., and Bolivar, F. G. (2004). Growth-rate recovery of *Escherichia coli* cultures carrying a multicopy plasmid, by engineering of the pentose-phosphate pathway. *Biotechnol. Bioeng.* 87 (4), 485–494. doi:10.1002/bit.20137
- Funke, M., Diederichs, S., Kensy, F., Müller, C., and Büchs, J. (2009). The baffled microtiter plate: Increased oxygen transfer and improved online monitoring in small scale fermentations. *Biotechnol. Bioeng.* 103 (6), 1118–1128. doi:10.1002/bit.22341
- Gawin, A., Valla, S., and Brautaset, T. (2017). The XylS/Pm regulator/promoter system and its use in fundamental studies of bacterial gene expression, recombinant protein production and metabolic engineering. *Microb. Biotechnol.* 10 (4), 702–718. doi:10.1111/1751-7915.12701
- Glick, B. R. (1995). Metabolic load and heterologous gene expression. *Biotechnol. Adv.* 13 (2), 247–261. doi:10.1016/0734-9750(95)00004-A
- Guo, A. C., Jewison, T., Wilson, M., Liu, Y., Knox, C., Djoumbou, Y., et al. (2012). Ecmdb: The *E. coli* metabolome database. *Nucleic Acids Res.* 41 (D1), D625–D630. doi:10.1093/nar/gks992

- Haddadin, F. T., and Harcum, S. W. (2005). Transcriptome profiles for high-cell-density recombinant and wild-type *Escherichia coli*. *Biotechnol. Bioeng.* 90 (2), 127–153. doi:10.1002/bit.20340
- Han, M. J., and Lee, S. Y. (2006). The *Escherichia coli* proteome: Past, present, and future prospects. *Microbiol. Mol. Biol. Rev.* 70 (2), 362–439. doi:10.1128/MMBR.00036-05
- Haugan, K., Karunakaran, P., Tondervik, A., and Valla, S. (1995). The host range of RK2 minimal replicon copy-up mutants is limited by species-specific differences in the maximum tolerable copy number. *Plasmid* 33 (1), 27–39. doi:10.1006/plas.1995.1004
- Hemmerich, J., Noack, S., Wiechert, W., and Oldiges, M. (2018). Microbioreactor systems for accelerated bioprocess development. *Biotechnol. J.* 13 (4), 1700141. doi:10.1002/biot.201700141
- Hoffmann, F., and Rinas, U. (2004). “Stress induced by recombinant protein production in *Escherichia coli*,” in *Physiological stress responses in bioprocesses. Advances in biochemical engineering* (Berlin, Heidelberg: Springer), Vol. 89, 73–92.
- Huang, C.-J., Peng, H.-L., Patel, A. K., Singhania, R. R., Dong, C.-D., and Cheng, C.-Y. (2021). Effects of lower temperature on expression and biochemical characteristics of HCV NS3 antigen recombinant protein. *Catalysts* 11 (11), 1297. doi:10.3390/catal11111297
- Hunter, J. D. (2007). Matplotlib: A 2D graphics environment. *Comput. Sci. Eng.* 9 (3), 90–95. doi:10.1109/mcse.2007.55
- Jeong, H., Kim, H. J., and Lee, S. J. (2015). Complete genome sequence of *Escherichia coli* strain BL21. *Genome* 3 (2), e00134. doi:10.1128/genomeA.00134-15
- Jeong, K. J., and Lee, S. Y. (2003). Enhanced production of recombinant proteins in *Escherichia coli* by filamentation suppression. *Appl. Environ. Microbiol.* 69 (2), 1295–1298. doi:10.1128/AEM.69.2.1295-1298.2003
- Jones, K. L., Kim, S. W., and Keasling, J. D. (2000). Low-copy plasmids can perform as well as or better than high-copy plasmids for metabolic engineering of bacteria. *Metab. Eng.* 2 (4), 328–338. doi:10.1006/mben.2000.0161
- Kaur, J., Kumar, A., and Kaur, J. (2018). Strategies for optimization of heterologous protein expression in *E. coli*: Roadblocks and reinforcements. *Int. J. Biol. Macromol.* 106, 803–822. doi:10.1016/j.ijbiomac.2017.08.080
- Kensy, F., Engelbrecht, C., and Buchs, J. (2009a). Scale-up from microtiter plate to laboratory fermenter: Evaluation by online monitoring techniques of growth and protein expression in *Escherichia coli* and *Hansenula polymorpha* fermentations. *Microb. Cell Fact.* 8, 68. doi:10.1186/1475-2859-8-68
- Kensy, F., Zang, E., Faulhammer, C., Tan, R.-K., and Büchs, J. (2009b). Validation of a high-throughput fermentation system based on online monitoring of biomass and fluorescence in continuously shaken microtiter plates. *Microb. Cell Factories* 8 (1), 31. doi:10.1186/1475-2859-8-31
- Kim, H. J., Kwon, Y. D., Lee, S. Y., and Kim, P. (2012). An engineered *Escherichia coli* having a high intracellular level of ATP and enhanced recombinant protein production. *Appl. Microbiol. Biotechnol.* 94 (4), 1079–1086. doi:10.1007/s00253-011-3779-0
- Kim, H., Kim, S., and Yoon, S. H. (2018). Metabolic network reconstruction and phenome analysis of the industrial microbe, *Escherichia coli* BL21(DE3). *PLOS ONE* 13 (9), e0204375. doi:10.1371/journal.pone.0204375
- Kim, S., Jeong, H., Kim, E.-Y., Kim, J. F., Lee, S. Y., and Yoon, S. H. (2017). Genomic and transcriptomic landscape of *Escherichia coli* BL21(DE3). *Nucleic Acids Res.* 45 (9), 5285–5293. doi:10.1093/nar/gkx228
- Kirk, O., Borchert, T. V., and Fuglsang, C. C. (2002). Industrial enzyme applications. *Curr. Opin. Biotechnol.* 13 (4), 345–351. doi:10.1016/S0958-1669(02)00328-2
- Konz, J. O., King, J., and Cooney, C. L. (1998). Effects of oxygen on recombinant protein expression. *Biotechnol. Prog.* 14 (3), 393–409. doi:10.1021/bp980021l
- Korz, D. J., Rinas, U., Hellmuth, K., Sanders, E. A., and Deckwer, W. D. (1995). Simple fed-batch technique for high cell density cultivation of *Escherichia coli*. *J. Biotechnol.* 39 (1), 59–65. doi:10.1016/0168-1656(94)00143-Z
- Kumar, J., Chauhan, A. S., Shah, R. L., Gupta, J. A., and Rathore, A. S. (2020). Amino acid supplementation for enhancing recombinant protein production in *E. coli*. *Biotechnol. Bioeng.* 117 (8), 2420–2433. doi:10.1002/bit.27371
- Kumar, K., Venkatraman, V., and Bruheim, P. (2021). Adaptation of central metabolite pools to variations in growth rate and cultivation conditions in *Saccharomyces cerevisiae*. *Microb. Cell Fact.* 20 (1), 64. doi:10.1186/s12934-021-01557-8
- Kunze, M., Roth, S., Gartz, E., and Büchs, J. (2014). Pitfalls in optical on-line monitoring for high-throughput screening of microbial systems. *Microb. Cell Factories* 13 (1), 53. doi:10.1186/1475-2859-13-53
- Kvitvang, H. F., and Bruheim, P. (2015). Fast filtration sampling protocol for mammalian suspension cells tailored for phosphometabolome profiling by capillary ion chromatography - tandem mass spectrometry. *J. Chromatogr. B Anal. Technol. Biomed. Life Sci.* 998–999, 45–49. doi:10.1016/j.jchromb.2015.06.018
- Kvitvang, H. F., Kristiansen, K. A., and Bruheim, P. (2014). Assessment of capillary anion exchange ion chromatography tandem mass spectrometry for the quantitative profiling of the phosphometabolome and organic acids in biological extracts. *J. Chromatogr. A* 1370, 70–79. doi:10.1016/j.chroma.2014.10.029
- Larentis, A. L., Nicolau, J. F., Esteves Gdos, S., Vareschini, D. T., de Almeida, F. V., dos Reis, M. G., et al. (2014). Evaluation of pre-induction temperature, cell growth at induction and IPTG concentration on the expression of a leptospiral protein in *E. coli* using shaking flasks and microbioreactor. *BMC Res. Notes* 7, 671. doi:10.1186/1756-0500-7-671
- Lempp, M., Lubrano, P., Bange, G., and Link, H. (2020). Metabolism of non-growing bacteria. *Biol. Chem.* 401 (12), 1479–1485. doi:10.1515/hsz-2020-0201
- Li, Z., Nimtz, M., and Rinas, U. (2017). Global proteome response of *Escherichia coli* BL21 to production of human basic fibroblast growth factor in complex and defined medium. *Eng. Life Sci.* 17 (8), 881–891. doi:10.1002/elsc.201700036
- Li, Z., and Rinas, U. (2021). Recombinant protein production-associated metabolic burden reflects anabolic constraints and reveals similarities to a carbon overfeeding response. *Biotechnol. Bioeng.* 118 (1), 94–105. doi:10.1002/bit.27553
- Liu, M., Feng, X., Ding, Y., Zhao, G., Liu, H., and Xian, M. (2015). Metabolic engineering of *Escherichia coli* to improve recombinant protein production. *Appl. Microbiol. Biotechnol.* 99 (24), 10367–10377. doi:10.1007/s00253-015-6955-9
- Losén, M., Frolich, B., Pohl, M., and Buchs, J. (2004). Effect of oxygen limitation and medium composition on *Escherichia coli* fermentation in shake-flask cultures. *Biotechnol. Prog.* 20 (4), 1062–1068. doi:10.1021/bp034282t
- Lozano Terol, G., Gallego-Jara, J., Sola Martínez, R. A., Martínez Vivancos, A., Cánovas Díaz, M., and de Diego Puente, T. (2021). Impact of the expression system on recombinant protein production in *Escherichia coli* BL21. *Front. Microbiol.* 12, 682001. doi:10.3389/fmicb.2021.682001
- Lu, W., Su, X., Klein, M. S., Lewis, I. A., Fiehn, O., and Rabinowitz, J. D. (2017). Metabolite measurement: Pitfalls to avoid and practices to follow. *Annu. Rev. Biochem.* 86, 277–304. doi:10.1146/annurev-biochem-061516-044952
- Mairhofer, J., Scharl, T., Marisch, K., Cserjan-Puschmann, M., and Striedner, G. (2013). Comparative transcription profiling and in-depth characterization of plasmid-based and plasmid-free *Escherichia coli* expression systems under production conditions. *Appl. Environ. Microbiol.* 79 (12), 3802–3812. doi:10.1128/AEM.00365-13
- Martins, A. C., Oshiro, M. Y., Albericio, F., de la Torre, B. G., Pereira, G. J. V., and Gonzaga, R. V. (2022). Trends and perspectives of biological drug approvals by the fda: A review from 2015 to 2021. *Biomedicines* 10 (9), 2325. doi:10.3390/biomedicines10092325
- Mesbah, N. M. (2022). Industrial biotechnology based on enzymes from extreme environments. *Front. Bioeng. Biotechnol.* 10, 870083. doi:10.3389/fbioe.2022.870083
- Muhamadali, H., Xu, Y., Morra, R., Trivedi, D. K., Rattray, N. J. W., Dixon, N., et al. (2016). Metabolomic analysis of riboswitch containing *E. coli* recombinant expression system. *Mol. Biosyst.* 12 (2), 350–361. doi:10.1039/C5MB00624D
- Muhlmann, M., Forsten, E., Noack, S., and Buchs, J. (2017). Optimizing recombinant protein expression via automated induction profiling in microtiter plates at different temperatures. *Microb. Cell Fact.* 16 (1), 220. doi:10.1186/s12934-017-0832-4
- Neidhardt, F. C., Ingraham, J. L., and Schaechter, M. (1990). *Physiology of the bacterial cell: A molecular approach*. Sinauer Associates.
- Ou, J., Wang, L., Ding, X., Du, J., Zhang, Y., Chen, H., et al. (2004). Stationary phase protein overproduction is a fundamental capability of *Escherichia coli*. *Biochem. Biophys. Res. Commun.* 314 (1), 174–180. doi:10.1016/j.bbrc.2003.12.077
- Overton, T. W. (2014). Recombinant protein production in bacterial hosts. *Drug Discov. Today* 19 (5), 590–601. doi:10.1016/j.drudis.2013.11.008
- Ow, D. S.-W., Nissom, P. M., Philp, R., Oh, S. K.-W., and Yap, M. G.-S. (2006). Global transcriptional analysis of metabolic burden due to plasmid maintenance in *Escherichia coli* DH5 α during batch fermentation. *Enzyme Microb. Technol.* 39 (3), 391–398. doi:10.1016/j.enzymictec.2005.11.048
- Özkan, P., Sariyar, B., Ütkür, F. Ö., Akman, U., and Hortaçsu, A. (2005). Metabolic flux analysis of recombinant protein overproduction in *Escherichia coli*. *Biochem. Eng. J.* 22 (2), 167–195. doi:10.1016/j.bej.2004.09.012
- Pang, Z., Chong, J., Zhou, G., de Lima Morais, D. A., Chang, L., Barrette, M., et al. (2021). MetaboAnalyst 5.0: Narrowing the gap between raw spectra and functional insights. *Nucleic Acids Res.* 49 (W1), W388–W396. doi:10.1093/nar/gkab382
- Philip, P., Kern, D., Goldmanns, J., Seiler, F., Schulte, A., Habicher, T., et al. (2018). Parallel substrate supply and pH stabilization for optimal screening of *E. coli* with the membrane-based fed-batch shake flask. *Microb. Cell Fact.* 17 (1), 69. doi:10.1186/s12934-018-0917-8
- Phue, J. N., and Shiloach, J. (2005). Impact of dissolved oxygen concentration on acetate accumulation and physiology of *E. coli* BL21, evaluating transcription levels of key genes at different dissolved oxygen conditions. *Metab. Eng.* 7 (5–6), 353–363. doi:10.1016/j.ymben.2005.06.003
- Puetz, J., and Wurm, F. M. (2019). Recombinant proteins for industrial versus pharmaceutical purposes: A review of process and pricing. *Processes* 7 (8), 476. doi:10.3390/pr7080476
- Roels, J. A. (1981). Application of macroscopic principles to microbial metabolism. *Ann. N. Y. Acad. Sci.* 369, 113–134. doi:10.1111/j.1749-6632.1981.tb14182.x
- Rosano, G. L., and Ceccarelli, E. A. (2014). Recombinant protein expression in *Escherichia coli*: Advances and challenges. *Front. Microbiol.* 5, 172–217. doi:10.3389/fmicb.2014.00172
- Rosano, G. L., Morales, E. S., and Ceccarelli, E. A. (2019). New tools for recombinant protein production in *Escherichia coli*: A 5-year update. *Protein Sci.* 28 (8), 1412–1422. doi:10.1002/pro.3668

- Røst, L. M., Brekke Thorfinnsdottir, L., Kumar, K., Fuchino, K., Eide Langørgen, I., Bartosova, Z., et al. (2020a). Absolute quantification of the central carbon metabolome in eight commonly applied prokaryotic and eukaryotic model systems. *Metabolites* 10 (2), 74. doi:10.3390/metabo10020074
- Røst, L. M., Shafaei, A., Fuchino, K., and Bruheim, P. (2020b). Zwitterionic HILIC tandem mass spectrometry with isotope dilution for rapid, sensitive and robust quantification of pyridine nucleotides in biological extracts. *J. Chromatogr. B Anal. Technol. Biomed. Life Sci.* 1144, 122078. doi:10.1016/j.jchromb.2020.122078
- Sanchez-Trasviña, C., Flores-Gatica, M., Enriquez-Ochoa, D., Rito-Palomares, M., and Mayolo-Deloso, K. (2021). Purification of modified therapeutic proteins available on the market: An analysis of chromatography-based strategies. *Front. Bioeng. Biotechnol.* 9, 717326. doi:10.3389/fbioe.2021.717326
- Sanden, A. M., Prytz, I., Tubulekas, I., Forberg, C., Le, H., Hektor, A., et al. (2003). Limiting factors in *Escherichia coli* fed-batch production of recombinant proteins. *Biotechnol. Bioeng.* 81 (2), 158–166. doi:10.1002/bit.10457
- Sevastyanovich, Y. R., Alfasi, S. N., and Cole, J. A. (2010). Sense and nonsense from a systems biology approach to microbial recombinant protein production. *Biotechnol. Appl. Biochem.* 55 (1), 9–28. doi:10.1042/BA20090174
- Sharma, A. K., Phue, J., Khatipov, E., Dalal, N., Anderson, E. D., and Shiloach, J. (2020). Effect of restricted dissolved oxygen on expression of *Clostridium difficile* toxin A subunit from *E. coli*. *Sci. Rep.* 10 (1), 3059. doi:10.1038/s41598-020-59978-1
- Silva, F., Queiroz, J. A., and Domingues, F. C. (2012). Evaluating metabolic stress and plasmid stability in plasmid DNA production by *Escherichia coli*. *Biotechnol. Adv.* 30 (3), 691–708. doi:10.1016/j.biotechadv.2011.12.005
- Simensen, V., Schulz, C., Karlsen, E., Brateland, S., Burgos, I., Thorfinnsdottir, L. B., et al. (2022). Experimental determination of *Escherichia coli* biomass composition for constraint-based metabolic modeling. *PLoS One* 17 (1), e0262450. doi:10.1371/journal.pone.0262450
- Singha, T. K., Gulati, P., Mohanty, A., Khasa, Y. P., Kapoor, R. K., and Kumar, S. (2017). Efficient genetic approaches for improvement of plasmid based expression of recombinant protein in *Escherichia coli*: A review. *Process Biochem.* 55, 17–31. doi:10.1016/j.procbio.2017.01.026
- Sletta, H., Nedal, A., Aune, T. E., Hellebust, H., Hakvag, S., Aune, R., et al. (2004). Broad-host-range plasmid pJB658 can be used for industrial-level production of a secreted host-toxic single-chain antibody fragment in *Escherichia coli*. *Appl. Environ. Microbiol.* 70 (12), 7033–7039. doi:10.1128/AEM.70.12.7033-7039.2004
- Sletta, H., Tondervik, A., Hakvag, S., Aune, T. E., Nedal, A., Aune, R., et al. (2007). The presence of N-terminal secretion signal sequences leads to strong stimulation of the total expression levels of three tested medically important proteins during high-cell-density cultivations of *Escherichia coli*. *Appl. Environ. Microbiol.* 73 (3), 906–912. doi:10.1128/AEM.01804-06
- Stafsnes, M. H., Røst, L. M., and Bruheim, P. (2018). Improved phosphometabolome profiling applying isotope dilution strategy and capillary ion chromatography-tandem mass spectrometry. *J. Chromatogr. B Anal. Technol. Biomed. Life Sci.* 1083, 278–283. doi:10.1016/j.jchromb.2018.02.004
- Sutay Kocabas, D., and Grumet, R. (2019). Evolving regulatory policies regarding food enzymes produced by recombinant microorganisms. *Gm. Crops Food* 10 (4), 191–207. doi:10.1080/21645698.2019.1649531
- Szenk, M., Dill, K. A., and de Graff, A. M. R. (2017). Why do fast-growing bacteria enter overflow metabolism? Testing the membrane real estate hypothesis. *Cell Syst.* 5 (2), 95–104. doi:10.1016/j.cels.2017.06.005
- Taymaz-Nikerel, H., Borujeni, A. E., Verheijen, P. J. T., Heijnen, J. J., and van Gulik, W. M. (2010). Genome-derived minimal metabolic models for *Escherichia coli* MG1655 with estimated *in vivo* respiratory ATP stoichiometry. *Biotechnol. Bioeng.* 107 (2), 369–381. doi:10.1002/bit.22802
- Terpe, K. (2006). Overview of bacterial expression systems for heterologous protein production: From molecular and biochemical fundamentals to commercial systems. *Appl. Microbiol. Biotechnol.* 72 (2), 211–222. doi:10.1007/s00253-006-0465-8
- Thorfinnsdottir, L. B., García-Calvo, L., Bø, G. H., Bruheim, P., and Røst, L. M. (2023). Optimized fast filtration-based sampling and extraction enables precise and absolute quantification of the *Escherichia coli* central carbon metabolome. *Metabolites* 13 (2), 150. doi:10.3390/metabo13020150
- Tripathi, N. K., and Shrivastava, A. (2019). Recent developments in bioprocessing of recombinant proteins: Expression hosts and process development. *Front. Bioeng. Biotechnol.* 7, 420. doi:10.3389/fbioe.2019.00420
- Veit, A., Polen, T., and Wendisch, V. F. (2007). Global gene expression analysis of glucose overflow metabolism in *Escherichia coli* and reduction of aerobic acetate formation. *Appl. Microbiol. Biotechnol.* 74 (2), 406–421. doi:10.1007/s00253-006-0680-3
- Waegeman, H., and Soetaert, W. (2011). Increasing recombinant protein production in *Escherichia coli* through metabolic and genetic engineering. *J. Ind. Microbiol. Biotechnol.* 38 (12), 1891–1910. doi:10.1007/s10295-011-1034-4
- Walsh, G. (2018). Biopharmaceutical benchmarks 2018. *Nat. Biotechnol.* 36 (12), 1136–1145. doi:10.1038/nbt.4305
- Weber, J., Hoffmann, F., and Rinas, U. (2002). Metabolic adaptation of *Escherichia coli* during temperature-induced recombinant protein production: 2. Redirection of metabolic fluxes. *Biotechnol. Bioeng.* 80 (3), 320–330. doi:10.1002/bit.10380
- Weber, J., Li, Z., and Rinas, U. (2021). Recombinant protein production provoked accumulation of ATP, fructose-1,6-bisphosphate and pyruvate in *E. coli* K12 strain TG1. *Microb. Cell Fact.* 20 (1), 169. doi:10.1186/s12934-021-01661-9
- Wittmann, C., Weber, J., Betiku, E., Krömer, J., Böhm, D., and Rinas, U. (2007). Response of fluxome and metabolome to temperature-induced recombinant protein synthesis in *Escherichia coli*. *J. Biotechnol.* 132 (4), 375–384. doi:10.1016/j.jbiotec.2007.07.495
- Worsey, M. J., and Williams, P. A. (1975). Metabolism of toluene and xylenes by *Pseudomonas putida* (arvilla) mt-2: Evidence for a new function of the TOL plasmid. *J. Bacteriol.* 124 (1), 7–13. doi:10.1128/jb.124.1.7-13.1975
- Wu, G., Yan, Q., Jones, J. A., Tang, Y. J., Fong, S. S., and Koffas, M. A. G. (2016). Metabolic burden: Cornerstones in synthetic biology and metabolic engineering applications. *Trends Biotechnol.* 34 (8), 652–664. doi:10.1016/j.tibtech.2016.02.010